E. S. Gevorkyan, V. P. Nerubatskyi

TECHNOLOGICAL AND SCIENTIFIC ASPECTS OF CONSOLIDATION OF REFRACTORY COMPOSITES

Monograph

MINISTRY OF SCIENCE AND EDUCATION OF UKRAINE

UKRAINIAN STATE UNIVERSITY OF RAILWAY TRANSPORT

E. S. Gevorkyan, V. P. Nerubatskyi

TECHNOLOGICAL AND SCIENTIFIC ASPECTS OF CONSOLIDATION OF REFRACTORY COMPOSITES

Monograph

Recommended by the Academic Council of Ukrainian State University
of Railway Transport

Kharkiv – 2022

UDC 621.763
G27

***Reviewers*:**

Rucki Mirosław, Dr. Habilitated Eng., Professor of Faculty of Mechanical Engineering of Kazimierz Pulaski University of Technology and Humanities in Radom;

Lytovchenko Serhii Volodymyrovych, Doctor of Engineering Sciences, Professor, Head of the Department of Materials for Reactor Building and Physical Technologies of V. N. Karazin Kharkiv National University;

Shabanova Halyna Mykolayivna, Doctor of Engineering Sciences, Professor of the Department of Ceramic, Refractory, Glass and Enamel Technologies of National Technical University "Kharkiv Polytechnic Institute".

Recommended by the Academic Council of Ukrainian State University of Railway Transport for publishing as monograph of June 17, 2022, report no. 3

G27 Gevorkyan E. S., Nerubatskyi V. P. Technological and scientific aspects of consolidation of refractory composites: Monograph. – Kharkiv: LLC "Voskhod-Print", 2022. – 73 p.
ISBN 978-617-8195-31-1

The monograph deals with modern methods for consolidation of powder mixtures based on refractory carbides, oxides and nitrides. Special attention is given to problems of compaction and consolidation of nanopowder mixtures based on refractory compounds. The monograph also presents the comparative characteristics of consolidation conducted with different methods, including the authors' techniques for highly effective electroconsolidation, which, despite its similarity to the technological SPS-process, has some distinguishing characteristics that simplify the production process, decrease the cost and guarantee lower initial cost of the finished goods. It also describes the comparative operational properties of the different materials obtained and used for wear resistant and abrasive tools and nozzles.

29 figures, 12 tables, 82 references

UDC 621.763

ISBN 978-617-8195-31-1

CONTENTS

ABBREVIATIONS AND NOMENCLATURE

AWJ – Abrasive Waterjet
FAST – Field Activated Sintering Technique
HVP – Hot Vacuum Pressing
SPS – Spark Plasma Sintering

INTRODUCTION

The technological compaction of powder mixtures is of primary importance for development and production of various composite materials. The fabrication methods and the sizes of initial powders in the composite mixture can vary from several dozens of microns to nanoscales. Only dense and non-porous materials can possess good physical and mechanical properties. Compaction of powder mixtures, the so-called consolidation, depends on numerous factors, the most important of which are the original grain size in a mixture, sintering temperature, sintering pressure and sintering environment. Among the technological consolidation processes for powder mixtures, especially, for ones produced from refractory ceramics (alumina oxide, zirconium oxide, silicon carbide, titanium carbide), the most efficient processes are hot pressing, cold and hot vibratory, pulse-magnetic and others characterized by a simultaneous impact of temperature and pressure. The finer is the grain size, the higher quality of dense materials can be obtained at a relatively lower temperature. However, it should be taken into account that hot pressing runs in special graphite press molds, and hot isostatic pressing – in special containers. It makes the technological process much more expensive, and the costs of the finished goods increase. With the introduction of the technology for fabricating nanopowders the issue of initial costs is becoming far more important, because the cost of the powders and their mixtures are rather high. And the consolidation process should not accelerate the grain growth so that to maintain the microstructure at the nano- or the submicron level for the composite obtained.

This monograph is part of the scientific project “The Use of Non-traditional Methods of Obtaining Nanopowders and Sintering for the Development of Modified Mullite-ZrO_2 Ceramics Resistant to Heat Shock” (State Registration No. 0121U109441). The monograph was prepared at the Department of Wagon Engineering and Product Quality of Ukrainian State University of Railway Transport (Kharkiv). The project is being implemented according to the competition held by the Ministry of Education and Science of Ukraine for projects on fundamental and applied scientific investigations, scientific and technical developments presented by higher educational establishments and academic institutions belonging to the Ministry of Education and Science of Ukraine as the budget program “Scientific and Research-and-Engineering Activity of Higher Educational Establishments and Academic Institutions”.

CHAPTER 1

SPECIAL FEATURES OF FABRICATING MATERIALS FROM NANODISPERSE AND SUBMICRON POWDERS OF REFRACTORY COMPOUNDS

1.1. Classification and analysis of known techniques for fabricating refractory nanopowders

Widely used modern powder production technologies are characterized by their resource and energy effectiveness as well as good ecological characteristics. The powder is an ensemble of individual solid bodies (or their aggregates) that contact with each other and have small sizes – from several nanometers to thousands of microns. In nanomaterial production the primary raw materials are ultradisperse powders the particle size of which is less than 100 nm and the powders obtained by intensive grinding that consist of grinded crystals.

Such powder technologies as pressing, sintering, hot pressing, etc. are used for obtaining a sample (product) of the set shapes and sizes with the appropriate structure and properties. The combination of these stages is often called *consolidation*. In terms of nanomaterials, consolidation must provide, on the one hand, practically full compaction (absence of macro- and micropores in the structure), and, on the other hand, maintenance of the nanostructure depending on the primary sizes of the ultradisperse powder (the grain size in sintered materials must be minimal, at least, less than 100 nm).

There are different methods for fabricating powders for nanomaterial production. They can be roughly divided into chemical and physical, the main of which with the most characteristic ultradisperse powders are given in table 1.1. However, this division is conventional. Thus, chemical reactions play an important role, for example, during evaporation in the media of reaction gases. At the same time, a lot of chemical methods are based on physical processes (low-temperature plasma, laser emission, etc.). As a rule, chemical methods are more universal and efficient, however the control over size, composition and form of particles is easier with physical methods, especially, condensational [1]. The ultradisperse particles in powders are mainly obtained by rapid heating (supersaturation) and reducing the pressure. Thus, we can see deposition from the gasous and liquid phases. However, during solid-phase synthesis, when kernels appear and grew, their crystalline lattices are re-built, and at high decomposing temperatures the particles that have been formed are sintered [2, 3].

Table 1.1 – Main methods of fabricating powders for nanomaterial production

Method	Method variant	Materials
Physical methods		
Evaporation and condensation	In vacuum or inactive gas	Zn, Cu, Ni, Al, Be, Sn, Pb, Mg, Ag, Cr, MgO, Al_2O_3, Y_2O_3, ZrO_2, SiC
	In reaction gas	TiN, AlN, ZrN, NbN, ZrO_2, Al_2O_3, TiO_2
High-energy fracture	Grinding	Fe–Cr, Be, Al_2O_3, TiC, Si_3N_4, NiAl, TiAl, AlN
	Detonation	BN, SiC, TiC, Fe, diamond
	Electric explosion	Al, Cd, Al_2O_3, TiO_2
Chemical methods		
Synthesis	Plasmo-chemical	TiC, TiN, Ti (C, N), VN, AlN, SiC, Si_3N_4, BN, W
	Laser	Si_3N_4, SiC, Si_3N_4–SiC
	Thermal	Fe, Cu, Ni, Mo, W, BN, TiC, WC–Co
	Self-propagating high-temperature	SiC, $MoSi_2$, AlN, TaC
	Mechano-chemical	TiC, TiN, NiAl, TiB_2, Fe–Cu, W–Cu
	Electro-chemical	WC, CeO_2, ZrO_2, WB_4
	Soluble	Mo_2C, BN, TiB_2, SiC
	Cryochemical	Ag, Pb, Mg, Cd
Thermal decomposition	Condensed precursors	Fe, Ni, Co, SiC, Si_3N_4, BN, AlN, ZrO_2, NbN
	Gaseous precursors	TiB_2, ZrB_2, BN

There are numerous methods for streamlining the synthesis processes in the appropriate direction. Sometimes the synthesis can be induced by means of the direct thermal decomposition method [4]:

– metal hydroxides;

– oxalates, acetates, sulphates, nitrates;

– main carbonates;

– ammonium sulphate obtained by hydrolysis of metal gluconates;

– settlement of organic acid salts;

– sol-gel method;

– lyophilisation; and

– spray-drying.

Complex compounds are produced from the primary mixtures with the given metal ions yielding to decomposition; the process includes several simultaneous solid-phase reactions forming a compound of the given composition. For simplicity only the formation of one solid phase is studied. It can happen that the phase that has been formed does not change, but it can form one or two new phases, which can lead to creation of a heterogeneous system. Solid-phase reactions are the process during which the numerous components of different composition interact with each other in the following combinations: solid–gas, solid–liquid, solid–solid, and during which a new solid phase is being formed.

The most promising synthesis method for nanopowders of refractory compounds is mechano-chemical synthesis, which can be used for production of nanocomposites, nanocrystalline powders of complex oxides and oxides of scattered elements with a particle size of 30...70 nm, which, in turn, are composed of blocks with the size of no more than 1…3 nm. The latter ones are used for fabricating nanostructural ferroelectric, piezoelectric and magnetic ceramics.

Among the unique methods for fabricating nanopowders are explosives. One of the most efficient and economical methods is the conductor electric explosion with subsequent condensation of the explosion products in the inert or specially designed gaseous environment. The research into this method has demonstrated that it can be used for fabricating nanodisperse Al_2O_3 powders with predominance of particles of less than 3 nm [5].

Another unique method for creating substances in the ultradisperse state is the explosive methods that can reach high thermodynamic parameters (temperature, pressure, etc.) over a short time. They are based on shock-wave compression and heating of the primary material; the particles obtained during the explosion are scattered and, interacting with the gaseous environment, rapidly get cool and form a nanopowder of the given composition. For example, it is a way that nanoparticles of Al, Mg, Ti, Zr, and Zn with the size from 5 to 10 nm are synthesized. There exist a lot of chemical methods for fabricating nanopowders. They are based on different phase transformations in liquid or steam. Among them are liquid supercooling, steam saturation, solid organic salt overheating, solubility limit exceeding, etc.

The plasmochemical method is a very effective way of fabricating nanodisperse powders. It is fulfilled on arc plasma facilities in which the arc, while burning between

anode and cathode, heats the gas flow up to several thousand degrees. And the gas can be of various compositions, either inert or any specified in advance. The plasmochemical method means that if a given material, even refractory, such as tungsten, tantalum, etc., is placed in the high-temperature gas, this material is subject to different transformation, from chemical to physical, in particular, condensation. All these transformations take extremely short periods – centiseconds or milliseconds. They accompany with an abrupt temperature fall to $10^5 \ldots 10^7$ degrees per second. And the material gets rapidly cool and crystallizes. It is possible to create the conditions under which this crystallization will have the form of nanoparticles. Thus, we can obtain a range of materials with the particle size from 10 to 100 nm.

The plasmochemical method for fabricating nanoparticles is highly efficient and can be used for fabricating nanopowders of various non-metal refractory compounds (particularly, solid alloys). For example, nanopowders of tungsten monocarbide, which are the basis of solid alloys, are produced with the previously prepared so-called precursors used for synthesis of WC nanopowders [6]. And they can be produced in existing furnaces where, with traditional methods, conventional powders are produced at much lower temperatures. If in traditional processes the temperature reaches 1200...1500 °C, in this case it is lower than 1000 °C. The fabrication of materials based on WC nanopowders is very promising. If the hardness of a tool increases 1.3...1.5 times, its strength rises in tens, consequently, application of such materials in production is very efficient.

The study of the nanopowders WC, NbC, TiC, SiC, Si_3N_4, AlN, and TaN obtained with the plasmochemical synthesis demonstrates that the general content of oxygen increases with a rise of the specific surface, and the main contribution in it is made by oxygen gases adsorbed on the surface [7].

1.2. Special features of fabricating composites from nano- and submicron powders

Conventional powder metallurgy uses powders with the particle size over 1 mkm, however, it is known, that, for example, the structural ceramic with high hardness and strength can be produced with as fine powder as possible. First of all, it decreases the sintering temperature and allows fabricating the fine structure, which gradually improves the physical and mechanical properties of the goods obtained. Of special interest is the field of research into the particles with the sizes from 100 nm to 1 mkm and less than 100 nm. An important task is to ensure a regular distribution of

densities of these nanodisperse powders in compacts of simple forms, to maintain the nanostructure in pressed forms for creating nanoscale grains by sintering, thus, to create the conditions that will inhibit the grain growth (to avoid recrystallization), and to sinter qualitative nanoceramic products with the given functional properties.

Study [8] presents some types of nanomaterials conveniently classified into consolidated objects, nanosemiconductors, nanoporous structures, nanopolymers, numerous nanotubular objects, nanobiomaterials, activators and supermolecular structures. The common thing for these materials is the size of the main structural components (crystallites, phase, pore, particle, molecular assemblies) generally not exceeding 100 nm.

The main technological methods for fabricating consolidated nanomaterials are given in table 1.2.

Table 1.2 – Main methods for fabricating consolidated nanomaterials

Method	Method variant	Objects
Powder technology	Gas-phase deposition and compaction (the Gleiter method). Conventional pressing and sintering. Electro-discharge sintering. Hot treatment with pressure (hot pressing, forging, extrusion)	Metals, alloys, compounds
Intensive plastic deformation	Torsional deformation at high pressures. Equal-channel angular pressing. Pressure processing of multilayer composites. Phase hardening	Metals and alloys
Controlled crystallization from the amorphous state	Crystallization at regular pressure. Crystallization at increased pressure	Amorphous substances
Technology of films and coatings	Chemical deposition from the gaseous phase. Physical deposition from the gaseous phase. Electric settling. Sol-gel technology	Metals, alloys, compounds

Table 1.2 also presents the most frequently used variants of these methods. It is evident that this classification is conventional, as the differences between some methods, as a rule, are not stark. Thus, during intensive plastic deformation or coating in the form of primary raw materials, powders are used; therefore, these methods can be considered as powder technologies. Also it is worthwhile to mention such methods

for fabricating nanostructures as irradiation with high doses of neurons and ions, intensive deformation during friction, etc. It is clear that each method has its own advantages and disadvantages. For example, powder technology methods do not always produce non-porous nanomaterials, however they are more universal regarding manufacturing products with different sizes and compositions. Controlled crystallization from the amorphous state, which provides fabricating non-porous samples, is restricted by the compositions that are capable of amorphisation. The methods given in table 1.2 do not contradict but complete each other and considerably expand the spectrum of structures, their properties and practical applications. A great diversity of methods for fabricating nanomaterials is one of the advantages of these objects.

There is a need to ensure the chemical purity and the required phase composition of the finished goods [9, 10].

Studies [11, 12], dedicated to the research into fabricating instrumental ceramics through reactive sintering of ultradisperse powders of chrome oxide and aluminium nitride obtained with the plasma-chemical synthesis method, demonstrate the prospects of the application of these powders for fabricating instrumental ceramics. With ultradisperse powders it is possible to reach a new level in terms of material properties and solve such an urgent problem as energy saving.

Obviously, the higher activities of fine powders obtained through plasma-chemical synthesis can decrease the sintering temperature and time, which is a transition to more economical temperature modes. Therefore, the issue of compaction and formation of nanodisperse and submicron powders is rather interesting.

Studies [13, 14] present deep and profound research into the main methods and peculiarities of fabricating new nanocomposite materials.

Studies [15, 16] describe the dimensional effects in consolidated nanomaterials. The authors explained interrelations between different properties and the characteristic dimensions of objects. Particularly, the following factors were determined:

– if the sizes of structural components decrease the interfaces become more important;

– the characteristics of the interfaces in the nanoscale interval can differ from those in conventional coarse-crystalline objects; and

– if the sizes of crystallites, particles and others decrease, their sizes become comparable with the characteristic values of some physical phenomena (e.g., length of the free run of carriers in the transport phenomena).

And successful research into the structures obtained from nano-disperse powders is based on the appropriate technological level and instrumentation. The study into the

nanomaterial structure is based on the methods of transmission electron microscopy, scanning electron microscopy and atomic-powder microscopy. A high resolution of electron microscopy methods is needed for identifying such features as presence of fine particles, pores and grains (less than 10…20 nm), monitoring dislocations, and determining the interfaces (boundaries of grains and phases), and also the fracture pattern for nanostructures.

The research into the dimensional particle range from 100 to 1000 nm is also of interest if taking into account that during sintering the sizes of the primary nanograins in the material can change due to the grain growth.

Study [17] presents the research into the special features of fabricating submicron particles by applying the vibrogrinding method. However, in this case the submicron size amounts to just 20 % out of the total powder mass, therefore, we cannot conclude about the properties of powders, especially at the submicron level (the grain size up to 1 mkm). Higher percentage of submicron powders is achieved by means of attrition grinding, however due to a great amount of particles with the size exceeding 1 mkm it is not possible to conclude about consolidation of particles with a size of up to 1 mkm. This dimensional range has not been studied enough, particularly, regarding refractory materials. At present two types of fine refractory ceramics are used as structural materials: oxide and oxygen-free.

Oxide ceramic performs well at high temperatures, it is flexible, well sinterable, however it cannot stand heating or cooling, thus it is thermally stable and strong.

Oxygen-free ceramics are the materials produced from powders of oxygen-free refractory compounds; they are thermal, corrosion and wear resistant.

Higher crack resistance of ceramics can be achieved through adding fine substances, alloying the ceramics, reinforcing them with high-strength crystallites or carbon threats, etc. [18].

Obviously, application of the nanopowder technology can be used for development of such fields:

– structural materials with high mechanical properties;

– materials for direct energy transformation – semiconductors, emission materials, materials for thermal pipes, and also superconductive materials La–Ba–Cu–O;

– activators for advanced petroleum refining and obtaining top quality petrol and gas;

– electrically-insulated, thermal-resistant and anti-corrosion coatings;

– materials for information registration systems;

– materials for water-power industry;

– composite materials of plastics and polymers with filler of ultradisperse powders;

– biologically active media for agriculture, biology and medicine; and

– porous structures for fine filters, brazing, welding and other purposes [19, 20].

1.3. Special features of fabricating high-density materials from nanodisperse powders of refractory compounds

High-density and porous ceramics are widely used in engineering. There exist traditional ways for fabricating high-density products from conventional powder mixtures; among them are hot pressing, high-temperature gas isostatic pressing, slip forming, injection molding, etc. However, some of these methods yield no result in case of nanopowders.

Table 1.3 presents some consolidation methods for nanodisperse powders.

Table 1.3 – Consolidation methods for nanocrystalline powders

Group	Name	Density, %	Grain size, nm
Consolidation in the rigid matrix	Hot pressing and hot-isostatic pressing	95	70…200
	High pressure sintering	4…98	50…100
	Electro-discharge sintering	95…97	30…80
	Impact-wave sintering	93…97	25…40
Pre-forming consolidation	Conventional sintering	99.5	120…200
	Sintering with controlled compaction speed	98.5…99.0	75…120
	Forge sintering	97…98.5	150…180
Free consolidation	Selective laser sintering	90…99	50…100
	Rapid prototyping	85…98	20…30

Most methods from table 1.3 are quick consolidation methods. They can be divided into consolidation of powders with the press mold and without it. The former ones are based on simultaneous application of pressure and temperature. Application of pressure can decrease the sintering temperature, shorten the high-temperature sintering and prevent the grain growth.

Table 1.4 gives some quick sintering methods.

Table 1.4 – Modern quick sintering methods for nanopowders

Consolidation method	Pressure, GPa	Temperature, °C	Product density, %	Heating rate	Hold time, s
Hot isostatic forge	less than 1.0	1200…1500	95	10…20	120…300
Quick hot isostatic pressing (QHIP)	0.5…1.0	1500	90	20…30	60…300
Field-activated sintering	less than 0.06	less than 2200	95	20…30	180…300
Electric sintering	less than 0.03	less than 3000	5…100	10…20	200
High-energy and quick compaction	1.5	3400	95	1…2	2
Super-high pressure sintering	26	2000	95	3…4	300…600

Table 1.4 shows that there exist a wide spectrum of consolidation methods for nanopowders, the most appropriate method for achieving the theoretical density of sintered nanopowders is the optimal choice between such parameters as temperature, pressure, oxidation-reduction reactions, voltage and current.

It should be noted that at present there has been intensive research in the field of consolidation of nanodisperse materials with application of electric fields, the so-called FAST (Field Activated Sintering Technique). This method is especially efficient for sintering boron carbide, silicon carbide, molybdenum disilicide, and alumina [21, 22].

Publications [23, 24] describe the efficiency of the FAST and SPS (Spark Plasma Sintering) methods. However, there exist some rather controversial conclusions regarding the processes running during sintering with application of these methods, particularly, ones of the structure formation mechanisms. For example, there is a hypothesis that plasma is being formed between the contacting nanopowders with the impulse current; it creates a strong connection between the particles [25, 26]. However, this hypothesis has not been verified yet. Particularly, there are some doubts about the

idea that a short-term impulse current intensifies the plasma-forming processes [27]. And so far this hypothesis has not been rejected yet.

An alternative method of consolidation for nanopowder materials has been offered by SuperGriphite (US) [28, 29]. This pressing method implies the passing of electric current through graphite powder (pressing environments) (fig. 1.1). The quasi-static pressure is simultaneously formed. The value of current reaches 10 A. With this method it is possible to produce goods of complex forms out of the pre-sintered so-called performs.

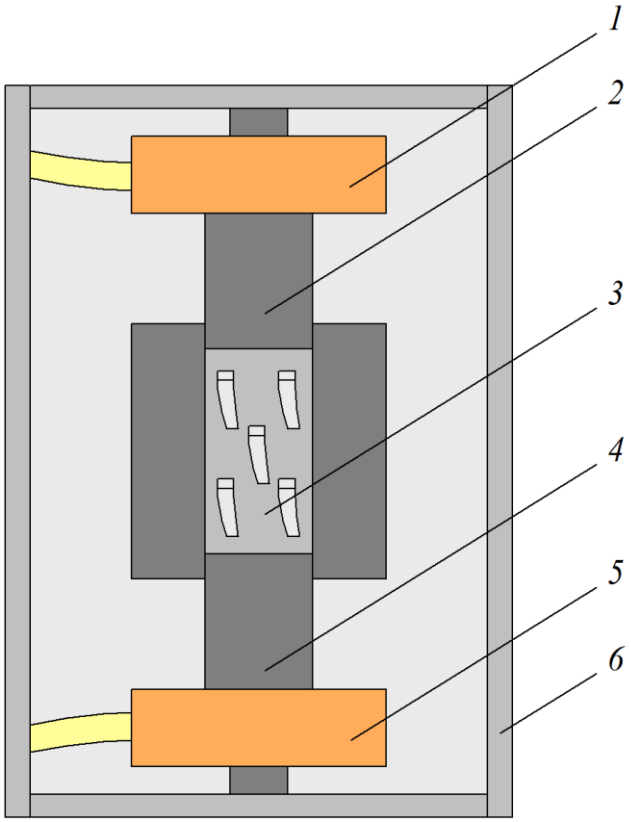

Figure 1.1 – Installation of powder electroconsolidation:
1 – top current conductor; *2* – top punch; *3* – matrix; *4* – bottom punch;
5 – bottom current conductor; *6* – vacuum chamber

The possibility to obtain goods of complex forms is an advantage. The most important technological operation in production of goods out of nanopowders is the formation of high-quality pressings (compacts) of the given form. One-phase nanopowders with multi-phase compositions (frequently very complicated) are characterized by metastable structural-phase state, developed specific surface and, consequently, high surface activity and capacity to agglomeration. As a rule, they are characterized by poor forming and pressing capacities due to their special physical and

chemical properties, particularly, high interparticle and wall friction (due to high specific surface), agglomeration of powders and a great amount of sorbed impurities. Therefore it is technologically difficult to ensure the regular density distribution in compacts of even a simple form out of such nanopowders and to maintain the nanostructure in compacts during sintering. The maintenance of the chemical purity and the required phase composition of finished goods are also of importance.

As known under the usual conditions of hot pressing the most important stage is final when compaction slows down, and for refractory oxides and carbides the main factor is the diffusion mechanism. For crystal materials the plastic deformation mechanism plays the leading role. The viscosity of substances is characterized by the yield point and with application of the voltage exceeding this value the so-called Bingham fluid is being created in the material [30]. It is assumed that the final compaction during hot pressing is the result of diffusion. The diffusion coefficient of the material obtained under pressure was calculated with the Coble model; it was much higher than that for the material obtained through conventional sintering, however the design value obtained by means of the Nabarro-Herring equation was very close to the value of the material sintered without pressure.

Naturally, the compaction process during hot sintering undergoes the following four stages:

– compaction speed is proportional to the logarithm of the pressure applied and depends on the grain sizes; it amounts to about 75 % out of the theoretical density;

– there appears the sliding and re-arranging of grains, and the material becomes more compacted under pressure; and

– plastic deformation starts on the grain contacts beginning with the second stage, and the compaction does not exceed 84 % out of the theoretical density.

The final stage includes compaction due to pressure diffusion. The compaction speed is higher than that during sintering without pressure and also depends on the surface energy.

Thus, if the conventional pressure applied a contribution of plastic deformation is small; it is the result of the diffusion activated by the pressure applied at the final stage.

Thus, we can assume that during compaction of nanodisperse powders the sliding along the grain boundaries is very important. Evidently, the compaction mechanism during hot pressing is rather complex and can be qualitatively assessed by means of additional research for each material, especially if it deals with such refractory compounds as tungsten monocarbide, silicon carbide, and alumina [31]. As for nanoparticles of these materials the mechanisms probably differ, and therefore, there

is a need for the further investigation into compaction of these particles during hot pressing. The issues of vacancy migration beyond the grain boundaries, particularly, during hot pressing of nanopowders are not enough studied, and identification of these processes can explain some patterns of their sintering.

In terms of efficiency and productiveness the hot pressing methods with application of electric current are the most efficient ones (table 1.5). The process is described with the term *electroconsolidation*, as the electric parameters in the description of this process are highly significant.

Table 1.5 – Comparative characteristics of some consolidation methods for nanopowders

Process	Sintering temperature, °C	Approximate size of a good, m	Compacting pressure, MPa	Complex details	Capital expenditures
Electroconsolidation	2500	0.20	70	yes	low
Quick hot isostatic pressing	2000	1.25	300	yes	very high
Ceracon	1500	0.40	400	difficult	average
Rapid Omnidirectional Compaction	1500	0.40	900	difficult	high

By their structural composition nanocomposite materials are divided into intra-, inter-, intra/inter- and nano/nano- types [32]. It is suggested that the first and second types are characterized by the disperse particle distribution of the second phase on or beyond the grain boundaries of the matrix phase. It is also characterized by improved hardness, crack resistance, strength both at the room or higher temperatures.

Nano/nano structural composite materials consist of the nanodisperse particles of both phases. This structure provides better mechanical properties mentioned above and such characteristics as machinability or high-temperature superplastic ductility similar to that of metal materials.

The most prospective field in the development of composite materials with ceramic matrixes is the fabrication of a composition of nano- and microcomposites, and also materials with the nano/nano-composite matrix additionally reinforced with

threadlike crystallites, micro-plates and/or disperse particles. Production of nanocomposite materials can include the traditional processes of powder metallurgy and ceramic technology, such as mixing of components, forming and further sintering without or with application of pressure, including hot isostatic pressing [33].

Formation of nanostructures considerably improves the mechanical properties of ceramic composite materials. For example, the strength of corundum ceramic is increased almost three times due to introduction of just 5 vol% of SiC nanoparticles into the ceramic matrix. An additional air or inactive-gas treatment increases the strength level up to 1500 MPa.

The introduction of the second phase and formation of the nanocomposite structure improve the mechanical properties of materials based on Al_2O_3, MgO and Si_3N_4. In the materials Al_2O_3–SiC and MgO–SiC the silicon carbide particles are located within the grains of the oxide phase [34]. The fracture pattern in these materials is a complete transcrystalline spall unlike a mixed inter- and transcrystalline destruction of matrix material (matrix samples). The transcrystalline fracture may be caused by the field of tensile residual stresses (over 1000 MPa) in the matrix around the disperse particles within the grains of the matrix. However, these stresses do not cause microcracking, as the size of SiC particles is much smaller than critical.

The electron-microscopic research has found formation of the subgrain dislocation structure within Al_2O_3 grains due to concentration of vacancies and dislocations. The annealing of this material at 1300 °C leads to the substructure development causing higher strength.

Composite materials have considerably higher strength values at higher temperatures. The transcrystalline fracture in nanocomposite materials is maintained up to 1000 °C and more. Disperse SiC particles (in Al_2O_3–SiC composite material) prevent the grain boundary sliding and the cavity formation within the matrix grains, and also slow down dislocations during deformation.

Nanocomposites Si_3N_4–SiC of mixed and interstructural type are very resistant to delayed fracture due to the subcritical crack propagation, as SiC particles located along the grain boundaries of silicon nitride slow down the average speed of crack propagation due to the high-temperature softening phase formed with sintered additives. Therefore, Si_3N_4–SiC composites maintain high strength at 1500 °C. At the same time Si_3N_4–SiC nanocomposites are superplastic at 1600 °C, particularly, if the α-Si_3N_4 modification is kept in the structure of the material.

Composite materials based on Si_3N_4 with the ultradisperse structure have higher creep resistance [35]. This effect is conditioned by the fixation of the grain boundaries with the particles of the second phase (SiC) preventing the grain intersliding and by the

change in the properties of the grain boundary phase due to interaction between carbon (for SiC particles) and the oxide additives added to activate sintering.

Reinforced composite materials are materials and alloys that have underformed high-disperse particles of refractory oxides, nitrides or carbides in their structure, which do not interact chemically with the matrix material and are specially added for reinforcement. The effect of reinforcing is proportional to the volume part of particles, and also their dispersity, which, at equal volume parts, determines the distance between the particles in the structure – the main reinforcing parameter for these materials. Reinforcement of disperse composite materials also depends on the matrix properties. The higher is its strength, the higher is the total strength of the whole material, all other things being equal.

Reinforced disperse composite materials are frequently produced with the methods of powder metallurgy or casting. The powder metallurgy methods use prepared components of composite materials in the form of powders or pellets of some sizes; they are weighted at a given ratio and equally mixed with each other. The samples are pressed out of the mixture and then sintered. Among the most famous reinforced disperse materials are alloys of sintered aluminium powder and sintered aluminium alloys produced of aluminium powder, with the Al_2O_3 film on the surface with the amount 5…25 % by volume. According to the thermal resistance level sintered aluminium powder and sintered aluminum alloys are preferable to high-strength aluminum alloys.

High strength and crack resistance of ceramics are achieved by means of effects of polymorphic transformations of zirconium dioxide with metastable tetragonal modification into stable monoclinic. This transformation is triggered by the external mechanical loads and causes nonrenewable consumption of energy for deformation and fracture of the material. In systems with disperse ZrO_2 particles unique materials have been produced with the bending strength over 1500 MPa and the crack resistance over 30 $MPa \cdot m^{-1/2}$. They also have higher resistance to subcritical crack growth and thermal stability [36, 37].

On the basis of the calculation of free surface energy in [38] the author has proposed the critical size; if the size is lower the properties change. For example, if it is lower than 5 nm, the catalyst activity rises, if it is lower than 20 nm, solid-magnetic materials become soft, if it is less than 50 nm, the thermal resistance changes, and if it is lower than 100 nm supermagnetism is achieved and conductivity grows. For example, it was found that if the expansion coefficient is lower than that of alumina, silicon carbide fabrics are compacted at lower temperature and pressure. The tangential stress around each particle is created in the matrix; it can prevent sporadic

intercrystalline fracture under the loading applied. High strength of the Al_2O_3–SiC system is achieved if the grain size is less than 50 nm.

The key factor for obtaining highly-disperse particles is the process of mixing and agglomeration of mixtures. Later on when the bonding is eliminated and the grain grows during consolidation, this process slows down due to the grains that still remain consolidated, because the strong transcrystalline bonding maintains. The mixing of powders greatly impacts the potential properties of nanocomposites and all composites. Different measures to improve the processes of fabricating mixtures are used; among them are different intensive methods of grinding, pyrolysis, sol-gel methods, chemical deposition, etc.

Study [39] details different evaporation mechanisms in composite materials. According to the research, the internal surface of a closed pore becomes the place of vacancy concentration, because for the concave form the curvature is negative. The pores turned into vacancies are dispersed in the sintered material and disappear in the area of the grain boundary. The grain boundary is considered as the division surface between the grains. This area has an excess disorder in the lattice. Therefore, this area is characterized by rapid migration of vacancies and their disappearance.

The pores can be eliminated through their division into vacancies, scattering across the lattice and removing from the sintered material [40]. With these boundaries the diffusion length of the vacancies near the pore becomes equal to the distance to the grain boundary (~ 1 mkm), and the pore collapse time shortens. Thus, grain boundaries provide formation of the fine and dense structure. With a rapid grain growth their boundaries migrate, but this process does not go with disappearance of vacancies and pores. The grain boundaries formed with big particles are curved, therefore the grain boundary moves towards particles with negative curvature, and big particles gradually grow. Thus, the particles grow abnormally. The grain boundaries move rapidly and the pores remain inside; thus, the process of formation of the fine and dense structure does not go.

However, it should be noted that the pore formation mechanisms described above clearly explain the processes going during sintering without pressure. But with a simultaneous application of pressure and temperature, particularly, if the temperature rises rapidly, it is easy to assume that pore formation, and, consequently, structure formation will be different. Fig. 1.2 presents the diagram of fabricating materials with the fine and dense structure during conventional sintering. Fabrication of materials with the density approximately up to 100 % requires the following:

– to use the particles with less than 1 mkm that have defects; and

– the particles must be approximately of similar size and form.

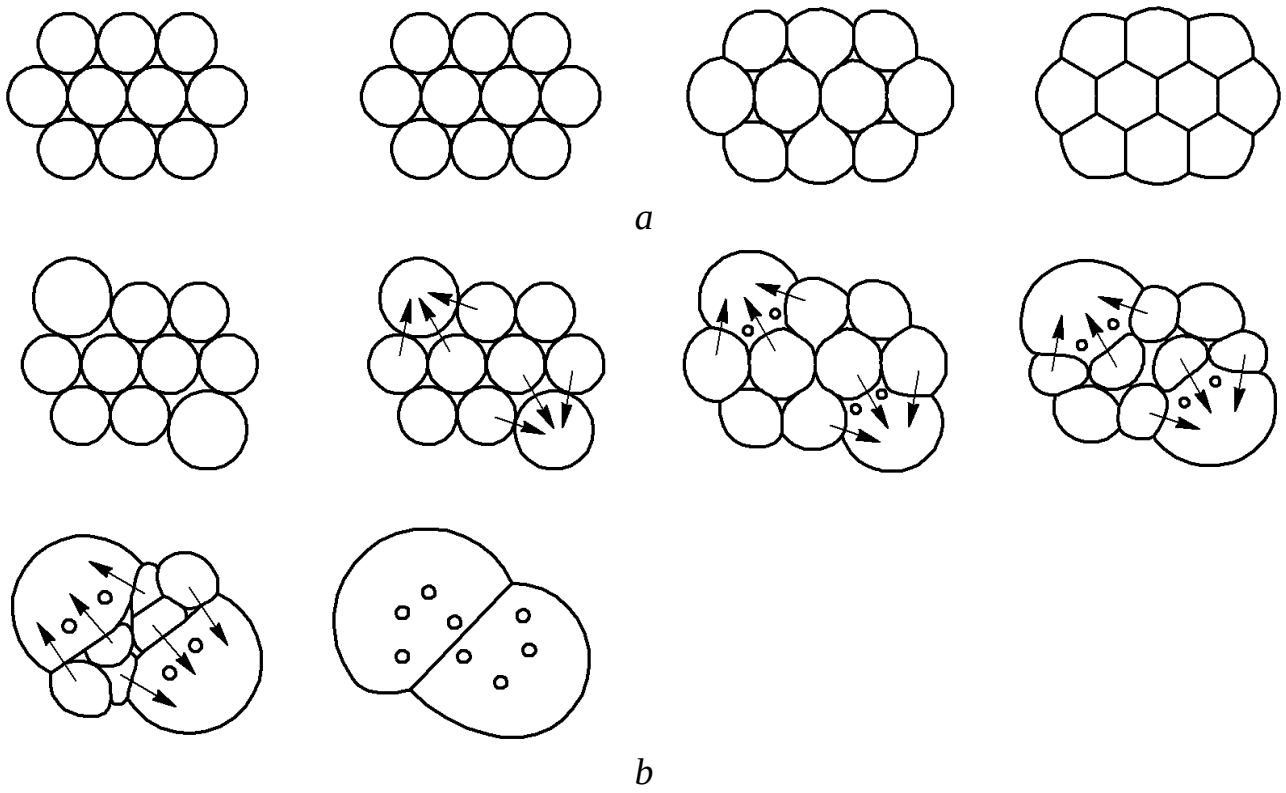

Figure 1.2 – Processes of fabricating materials with the fine and dense structure during sintering:
a – fixed grain boundaries, pores are turned into vacancies and disappear on the grain boundary; *b* – due to abnormal grain growth the pressing of the boundaries is high and pores remain inside the material (arrows indicate the direction of the pressing of the substances)

After mixing the mass should be formed. To limit the transfer of particles, another component for changing the phase composition in the area of grain boundaries is added.

The following types of sintering are used at present:

– sintering under the normal pressure (conventional);

– sintering under pressure (hot pressing – no mass production, graphite forms);

– sintering during isostatic pressing (hot isostatic pressing); and

– sintering during heating with electric current.

The last type mentioned can be divided into two types:

– indirect heating, particularly, inductive heating of graphite press molds; and

– direct heating when electric current goes through the powder being sintered.

Therefore, in terms of sintering with electric current it is of primary importance to study the issue of how the powder conducts electric current. If the powder does not conduct electric current, particularly, alumina, it is clear, that the current will go

through the graphite form rather than the powder, but as far as the resistance of graphite is low, the maximum current should be applied to heat the graphite form to high temperature. It is true for direct and impulse current. Most FAST methods use the impulse feed of electric current, which is the source of short-term plasma formation in the contact areas of nanoparticles. However, it should be assumed that application of alternative electric field initiates the Foucault currents in the graphite form, due to which the press mold and the powder, which is sintered, are additionally heated. Besides, alternative current forms alternative magnetic current that, most likely, can produce more regular and homogeneous density of the powders being sintered. In most cases lower sintering temperature and higher density of the material can be achieved through adding another component that forms the liquid phase during sintering. If formation of the liquid phase is undesirable the reaction sintering method can be used; it ensures the simultaneous processes of sintering and solid-phase reactions.

The method for obtaining powders is chosen according to physical and chemical criteria, and also, for most cases, profitability. Therefore, some methods for fabricating powders are just laboratory investigation.

Thus, despite numerous methods of sintering powders, the most efficient one, particularly, for sintering nano- and submicron powders of refractory compounds is the electroconsolidation method. Regarding the issues of sintering mechanisms and structure formation for various nanodisperse refractory compounds there exist a lot of ambiguous and disputable points, particularly, if it deals with the grain growth kinetics and the structure formation of refractory compound powders conducting and non-conducting electric current.

The WC material is still the most universal material for cutting tools and other wear resistant structural materials, such as stamps, press molds and different wear-resistant nozzles.

It is explained by such properties of this material as high hardness, strength, thermal stability, corrosion resistance and relatively high chemical inertia [41, 42]. At the same time electroconsolidation of nanodisperse powders of tungsten monocarbide has not been carefully studied yet.

CHAPTER 2

COMPACTION OF POWDERS WITH ELECTROCONSOLIDATION

2.1. Installation for electroconsolidation

The ceramic samples for the research were made with the hot pressing installation developed and produced at Ukrainian State University of Railway Transport. Its work is based on the FAST/SPS technology in which compaction is fulfilled through pressing the initial powder-like substance with simultaneous DC or AC heating.

Electric discharge in the contact area of powder particles can lead to clearing the surface and creating surface defects that accelerate the grain-boundary diffusion due to the additional free volume $\Delta\alpha$ [43]:

$$D_b(\alpha) \to D_b^* = D_b^*(\alpha + \Delta\alpha), \tag{2.1}$$

where $D_b(\alpha)$ – the conventional value of the coefficient of grain-boundary diffusion; α – the free volume of boundaries; D_b^* – the coefficient of grain-boundary diffusion in the theory of non-equilibrium grain boundaries.

The main components of the installation for electroconsolidation designed are vacuum hot-pressing chamber (fig. 2.1) of the volume 7 dm^3, power source (0…75 kVA, 50 Hz), and hydraulic press (0…12 t). Vacuum chamber *1* (fig. 2.1) has current conducting graphite press mold *6–8* with powder being compacted *9* between the current conductors. The air is pumped off the chamber to the pressure 10^{-3} Pa with a forvacuum pump NVR-4.5D. Later on the current source activates and the gradual heating begins.

The network transformer TVK-75 is used as a powerful power source; therefore, a volume of about 10 V at the current 3...9 kA is obtained on the secondary coil. Such heavy currents cause the inevitable heating of the contacts on the outside of the vacuum area. It can be eliminated by forced water-cooling of the external part of the vacuum chamber and by water-cooling of the flexible current conductors with which the installation is connected to the secondary coil.

The current going through the press mold and the batch is controlled with the power-controlling unit that regulates the current in the primary coil of the transformer. Therefore the temperature and the heating speed are controlled precisely, and adjustments to the sintering process can be made.

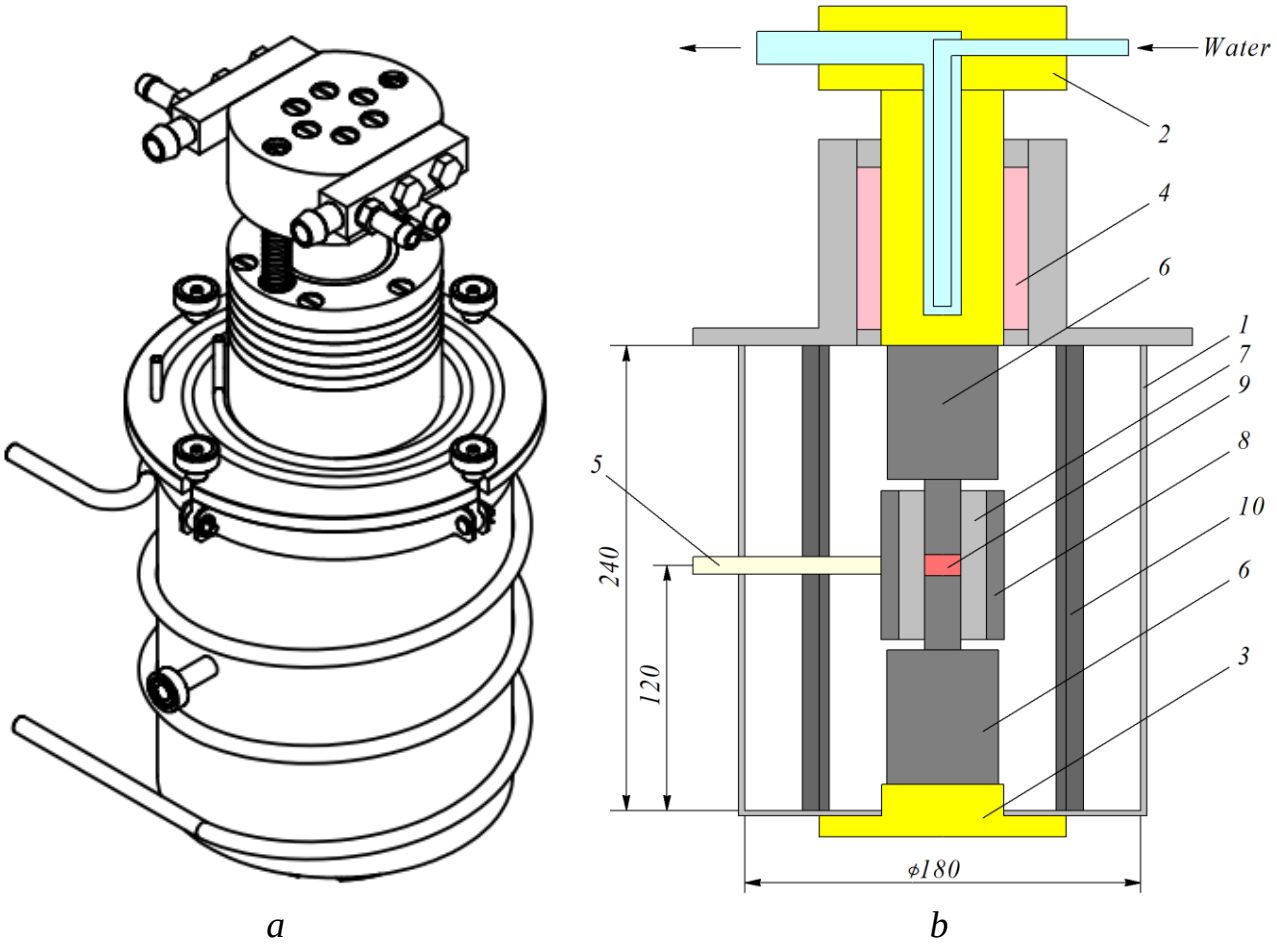

Figure 2.1 – General view (*a*) and the diagram (*b*) of the vacuum sintering chamber and the graphite press mold of the installation for electroconsolidation:
1 – body; *2*, *3* – top and bottom current conductors, respectively;
4 – compactor; *5* – thermal element; *6* – punches; *7* – matrix of the press mold;
8 – press mold shell; *9* – pressing zone; *10* – screen

According to the results obtained during the implementation of this installation we can state that the use of an AC power source with the industrial frequency (50 Hz), in fact, gives the same results as for a DC power source. But, unlike the impulse sources, this installation is not expensive, simple structurally, and, consequently, more reliable.

2.2. Measurement and registration of electroconsolidation parameters

More detailed information on the compaction process was obtained by means of the control measuring complex (fig. 2.2).

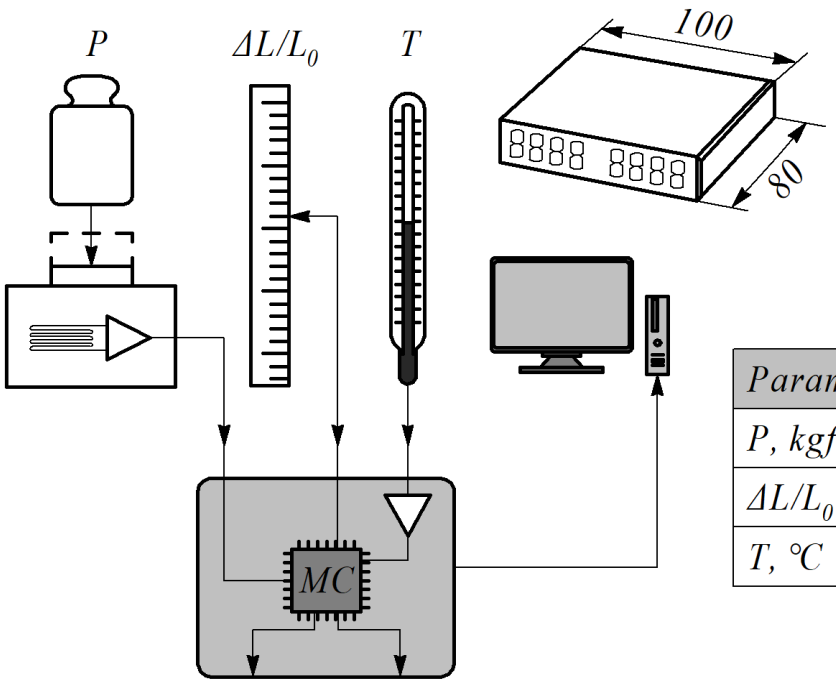

Parameter	Range	Step
P, kgf	0...1000	4.0
$\Delta L/L_0$, mm	0...300	0.07
T, ℃	20...2000	1.0

Figure 2.2 – System of registering devices of the hot pressing installation

The pressure was measured with the tension sensor designed and manufactured in advance; it transformed the mechanical stress into an electric signal. Its main components (fig. 2.3, *a*) were: unit of deformation *1*, strain-sensitive resisting elements *2*, and body *3*. The deformation unit was a metal hollow cylinder with the wide flat foundation of Steel 40X. Constantan wire-strain gauges were glued on the cylinder surface being deformed. They were connected according to the standard Wien bridge diagram. The sensors along the axis changed their resistance under pressure and disbalanced the bridge, the signal from which was reinforced with the special instrumental amplifier AD8221.

Considering a high sensitivity of the amplifier even constantan with the low resistance temperature drift ($3 \cdot 10^{-5}$ K^{-1}) created great differences of "0". In order to prevent this, similar wire sensors were used as opposite shoulders; they were glued in close proximity, but they did not participate in deformation of the foundation. The amplifier was mounted on a small printed plate of the size 31×23 mm located inside the strain gauge body.

The settling during pressing was recorded with a device monitoring the motion of the upper moving punch. It was built on the basis of an encoder strip fixed on the immovable part of the installation frame and an optical sensor moving along the strip together with the upper current conductor. By applying this approach it was possible to obtain the running accuracy 70 mkm in a wide range of positions without calibration, and the output signal was digital and did not require amplification.

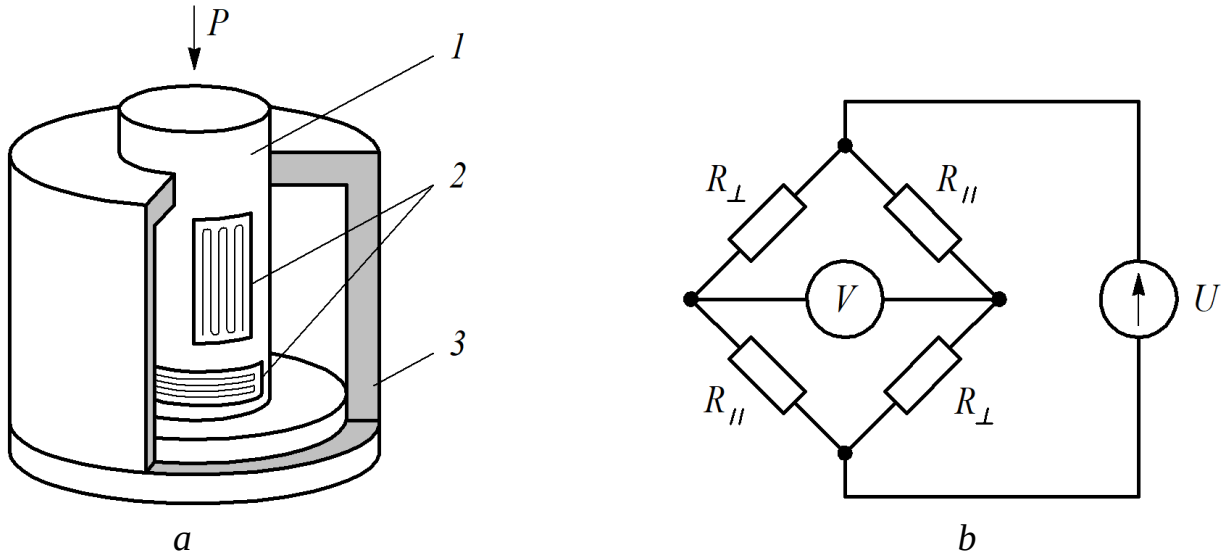

Figure 2.3 – Placement of the strain-sensing elements of a strain gauge (*a*) and the diagram of their connection (*b*)

The temperature was controlled on the peripheral part of the press mold with the tungsten-rhenium thermocouple VR-5/20, the signal from which was amplified with a precision operating amplifier. The calibration was made with an optical pyrometer. The precise temperature inside the pressing zone was calculated with mathematical modelling of the temperature distribution in the installation units with the finite element method.

The signals from each sensor were processed with the main device designed and manufactured on the basis of the AVR microcontroller. Each sensor was connected to the main block containing microcontroller, amplifier for the signal from the thermocouple, energy and reference sources, and couple of segment indicators. All these elements were placed in the compact body with the dimensions 100×80×20 mm.

Despite its small sizes, the main device could simultaneously record four parameters: pressure, temperature, displacement of the upper punch, and time. At a set interval the data were read from the sensors and on the real-time basis transferred to the computer that filed them for further processing and analysis. Part of the data (values of pressure and temperature) was transferred to the digital display on the frontal panel. The microcontroller had built-in software written in the programming language C in which the USB 2.0 interface was realized. This interface can be connected to any personal computer.

2.3. Methods of modelling thermal processes during electroconsolidation

The working part of the installation for hot vacuum pressing (HVP) has the axial symmetry. This part of the installation has the axial symmetry of electric and thermal fields; therefore the axisymmetric model with the cylindrical coordinate system can be used for their computer modelling. The computer model uses a half of the axial section of the working volume of the technological installation (fig. 2.4). During hot vacuum pressing the electric current with the industrial frequency 50 Hz is running in the installation. And when the current goes, Joule thermal sources appear in the conductivity elements of the installation and heat them. From the conductivity elements of the installation the heat is also transferred by means of thermal conductivity to the non-conducting elements, particularly, the powder workpiece. Besides, through emitting, the thermal energy is transferred from more heated elements of the installation to less heated ones.

For the modelling the electric and thermal fields in the working volume of the installations during sintering are used similarly [44]; the connected system of the equations of quasi-stationary electric conductivity is

$$div\left(\sigma(T)\,grad\,U\right)=0 \tag{2.2}$$

and non-stationary thermal conductivity is

$$c(T)\gamma(T)\frac{\partial T}{\partial t}=div\left(\lambda(T)\,grad\,T\right)+Q, \tag{2.3}$$

where U – the effective value of electric potential, $U = U(r, z, t)$; T – the temperature, $T = T(r, z, t)$; r, z – the cylindrical coordinates of the spatial point under study; t – the time; $\sigma(T)$, $c(T)$, $\gamma(T)$ and $\lambda(T)$ – the specific electric conductivity, thermal capacity, density and thermal conductivity coefficient, respectively; Q – the capacity of thermal sources.

The value Q according to Joule-Lenz's law is calculated according to the expression

$$Q=\sigma\left(T\right)\left(grad\,U\right)^2. \tag{2.4}$$

At the initial moment the conditions for the electric potential U and the temperature T are set:

$$U(r,z,0)=0, \tag{2.5}$$

$$T(r,z,0)=T_0, \tag{2.6}$$

where T_0 – the initial temperature.

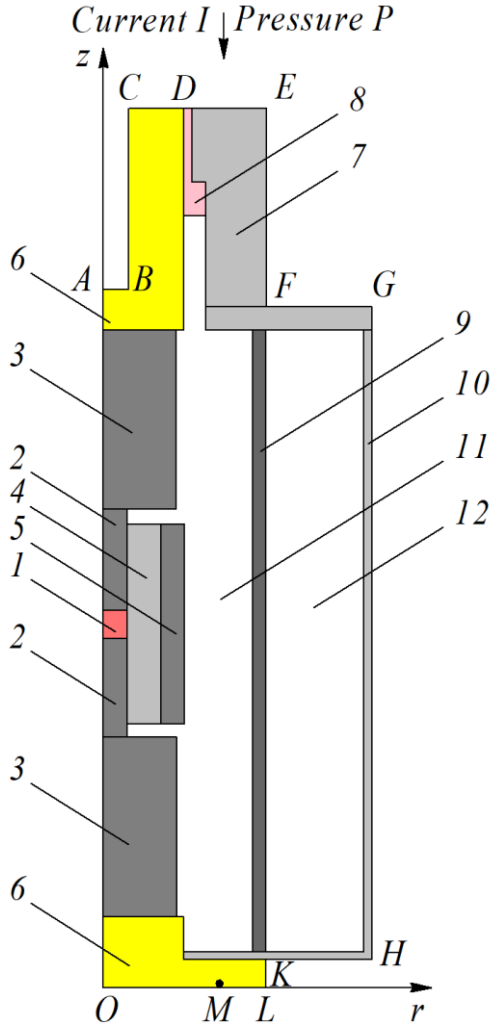

Figure 2.4 – Diagram of the technological installation of HVP
(half of the axial section):
1 – powder workpiece (Al_2O_3); *2* – graphite punches (MPG-7); *3* – graphite cylinders (MPG-7); *4* – press mold (MPG-7); *5* – shell (carbon-carbon composite material); *6* – current conductor (brass); *7* – duralumin (D16T); *8* – electric insulator (fluorine plastic); *9* – thermal display (thermally expanded graphite); *10* – chamber body (Steel 12Cr18N10T); *11*, *12* – vacuum cavities

The following boundary conditions in the electrical conductivity task are set. The voltage difference is applied to the surfaces *CD* and *OL* (fig. 2.4)

$$U(r,z,t)=u(t), \quad (r,z)\in CD, \tag{2.7}$$

$$U(r,z,t)=0, \quad (r,z)\in OL, \tag{2.8}$$

on the symmetry axis *Oz* (side *OA*) the symmetry condition is set

$$\frac{\partial U(r,z,t)}{\partial r}=0, \quad (r,z)\in OA, \tag{2.9}$$

and on the remaining surfaces of the structural elements of the design area, which has an access to the airspace, the following condition of failure of current (electric potential gradient) towards the surface normal is fulfilled:

$$\frac{\partial U(r,z,t)}{\partial n}=0. \tag{2.10}$$

The following boundary conditions for the thermal conductivity task are set. On the symmetry axis *OA* the symmetry condition of the thermal field is fulfilled similarly to (2.9):

$$\frac{\partial T(r,z,t)}{\partial r}=0, \quad (r,z)\in OA. \tag{2.11}$$

The surfaces *ABC* and *OM* are cooled with an intensive water flow of room temperature; therefore, during sintering their temperature is less than the steam point. The set conditions of convective thermal exchange on these surfaces are:

$$\lambda\frac{\partial T}{\partial n}(r,z,t)=\alpha_{ABC}(T)(T_C-T), \quad (r,z)\in(AB\cup BC), \tag{2.12}$$

$$\lambda\frac{\partial T}{\partial n}(r,z,t)=\alpha_{OL}(T)(T_C-T), \quad (r,z)\in OM, \tag{2.13}$$

where T_C – the environmental temperature; α_{ABC}, α_{OL} – the coefficients of convective thermal exchange on the corresponding surfaces; $\partial T/\partial n$ – the value of the derivative of the temperature towards the outward normal vector to the surface.

The conditions of the thermal exchange with the massive of plates from the press are set on the surfaces *CD*, *DE* and *ML*. These conditions are written on the basis of the thermal balance and by their form they are similar to the conditions of convective thermal exchange with the corresponding effective value α_{ef} of the coefficient of convective thermal exchange:

$$\lambda \frac{\partial T}{\partial n}(r,z,t) = \alpha_{ef}(T)(T_C - T), \quad (r,z) \in (CD \cup DE \cup ML). \tag{2.14}$$

The convective thermal exchange with the outer atmosphere on the external surface *EFGHKL* of the hot vacuum pressing installation is taken into account:

$$\lambda \frac{\partial T}{\partial n}(r,z,t) = \alpha_{air}(T)(T_C - T), \quad (r,z) \in EFGHKL, \tag{2.15}$$

where α_{air} – the coefficients of convective thermal exchange on this surface.

The thermal radiation heat transfer is conducted in each vacuum cavity *11* and *12* (fig. 2.4) of the hot vacuum pressing installation between the surfaces of its elements.

Equations [45, 46] are used for modelling the thermal radiation heat transfer between the surfaces $S_1, S_2, \ldots, S_{N_k}$

$$\sum_{i=1}^{N_k} \left(\frac{\delta_{ji}}{e_i} - F_{ji} \frac{1-e_i}{e_i} \right) \frac{Q_i}{A_i} = \sum_{i=1}^{N_k} \left(\delta_{ji} - F_{ji} \right) \sigma_S T_i^4, \quad k = 1,2,...,K, \tag{2.16}$$

$$Q_i = \sigma_S e_i F_{ij} A_i \left(T_i^4 - T_j^4 \right), \tag{2.17}$$

$$F_{ij} = \frac{1}{A_i} \int_{S_i} \int_{S_j} \frac{\cos\phi_i \cos\phi_j}{\pi r^2} dS_j \, dS_i, \tag{2.18}$$

they have been obtained on the basis of the equation of the thermal energy balance between these surfaces.

Expressions (2.14)…(2.17) use the following symbols: T_i, T_j – the absolute temperature of the *i*-th and the *j*-th surfaces, respectively; σ_S – the Stefan-Boltzmann

constant, $\sigma_S = 5{,}67 \cdot 10^{-8}$ W/(m^2·deg.^{4}); e_i – the emission coefficient of the *i*-th surface, $e_i = e_i(T)$; A_i – the square of the *i*-th surface, Q_i – the value of energy emitted by the *i*-th surface; δ_{ji} – the Kronecker delta; F_{ij} – the so-called angular coefficient, the numerical value of which equals the value of the energy emitted from the surface S_i and reached the surface S_j; r – the distance between the point P_i on the surface S_i and the point P_j on the surface S_j; φ_i – the angle between the vector $\overrightarrow{P_jP_i}$ and the normal to the surface S_i in the point P_i; φ_j – the angle between the vector $\overrightarrow{P_iP_j}$ and the normal to the surface S_j in the point P_j; N_k – the number of surfaces forming the *k*-th cavity and exchanging the thermal energy by means of emission between them; K – the number of cavities in which the heat is transferred by means of emission.

During the mathematic modelling of electric and thermal fields in the installation for sintering powders by means of heating with electric current, it is also important to take into account the conditions of contact between the elements of the installation on the contact surfaces, because these conditions impact the distribution of electric and temperature fields [47, 48]. These contact surfaces included in this research are given in fig. 2.5: H_1 and H_2 – the contact surfaces of the top punch with graphite cylinder and workpiece, respectively; H_3 and H_4 – the contact surfaces of the bottom punch with workpiece and graphite cylinder, respectively; V_1, V_2, V_3 and V_4 – the contact surfaces of the press mold with top punch, workpiece, bottom punch and shell, respectively. The transition through the contact surface towards the normal is accompanied with a leap of the corresponding field characteristics: electric potential and temperature.

On the contact surfaces the boundary contact conditions for electric and thermal conductivity tasks have the form

$$\sigma \frac{\partial U}{\partial n}\bigg|_1 = \sigma \frac{\partial U}{\partial n}\bigg|_2 = j_C, \qquad j_C = \sigma_C (U_2 - U_1), \tag{2.19}$$

$$\lambda \frac{\partial T}{\partial n}\bigg|_1 = \lambda \frac{\partial T}{\partial n}\bigg|_2 = q_C, \qquad q_C = \lambda_C (T_2 - T_1), \tag{2.20}$$

where the values with indexes *1* and *2* mean their values on both sides of the contact surface; $\sigma_C = \sigma_C(T, p)$ and $\lambda_C = \lambda_C(T, p)$ – the specific electric conductivity [Ohm^{-1}·m^{-2}] and the thermal conductivity coefficient [W/(m^2·deg)] of the contact surface, respectively; p – the pressure in the point under study on the contact surface.

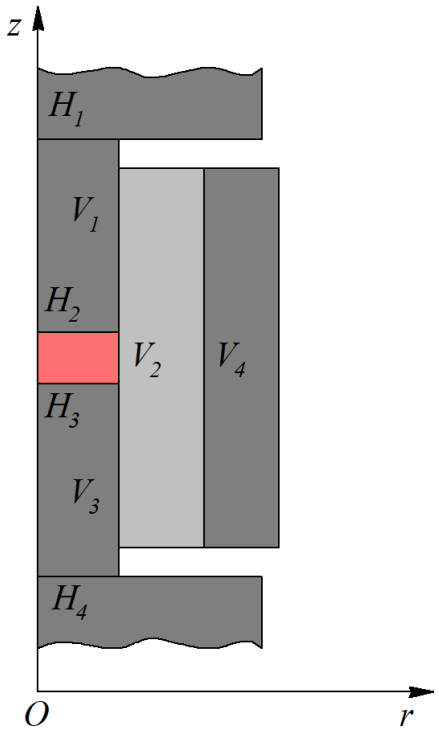

Figure 2.5 – Contact surfaces between the elements of the HVP installation on which the contact electric and thermal resistances are taken into account

Expressions (2.19) and (2.20) are written for the case when the normal vector to the contact surface is directed from medium *1* to medium *2*.

The computer-assisted realization of mathematical model (2.2)…(2.20) is conducted with the finite element method in combination with the radiosity method, and with the Newton-Raphson method by time. The computer modelling is made in ANSYS [49].

The spatial area is divided into 1438 finite elements (8-unit elements, square approximation) and 4477 units (fig. 2.6). In the areas with the forecast high gradients of electric potential and temperature the finite element mesh is clustered. The calculation time with the relative error 0.01 is 6…10 min.

The calculation was made with the following data. The sizes of the installation elements: the radius and the height of the workpiece are 10×10 mm; the lengths of graphite punches and cylinders are 36 and 65 mm, respectively; the external radius and the height of the press mold are 21 and 71 mm, respectively; the radius of the shell is 30 mm; the external radius and the thermal display thickness are 60 and 5 mm, respectively; the external radius and the body wall thickness are 97.5 and 1.0 mm, respectively. The other sizes can be determined according to the proportional ratios from fig. 2.4. The electric voltage 5 V is applied to the surfaces *CD* and *OL* of the brass electrodes. The working pressure is 35 MPa.

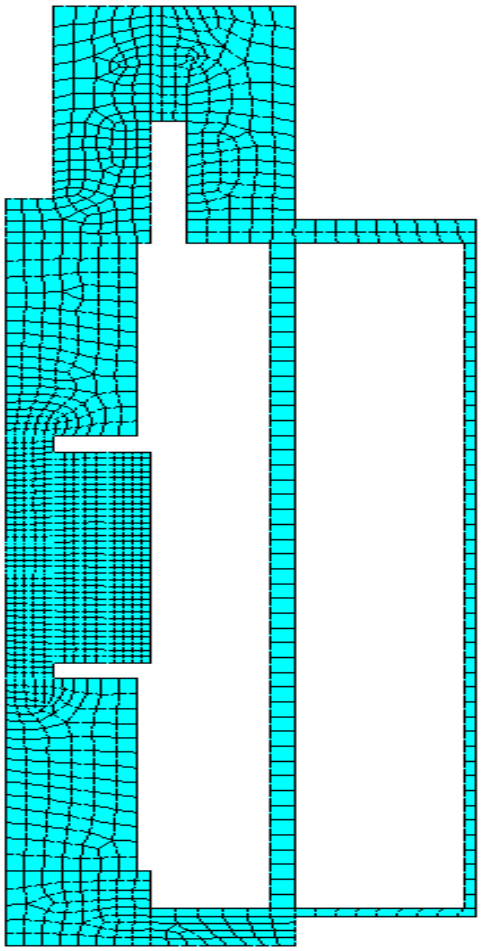

Figure 2.6 – Discretization of the spatial area to finite elements

The HVP process runs as follows: the first 1000 sec – heating at the set voltage, then – cooling over 500 sec without electric field. The calculation includes the temperature dependency of the material properties of the elements of the HVP installation obtained from [50, 51].

The values of the convective thermal exchange coefficients are chosen with the technique presented in [52].

The choice of the values of contact electric conductivities and thermal conductivities on the contact surfaces and their dependency on the temperature and pressing pressure is based on the analysis of the data given in [53, 54]. The contact electro- and thermal conductivities depend on many factors [55, 56]: roughness of the contact surfaces, thickness of the contact layer, square of the micro-irregularities of the contact surfaces, pressure and temperature in the contact points, orientation of the contact surface to the pressing force.

CHAPTER 3

PRODUCTION OF FINELY DISPERSED COMPOSITE MATERIALS FROM REFRACTORY COMPOUNDS WITH THE ELECTROCONSOLIDATION METHOD

3.1. Production of finely dispersed structures from tungsten monocarbide

Tungsten carbide as the basis of widely used solid alloys is of special attention among researchers in the field. The fabrication of the WC/Co nanopowders by means of low-temperature renovation and carbidization in the suspended layer of the mixture of ammonium meta-tungsten and cobaltic chloride with further spray drying (ensures good mixing of nano-components) has not been widely used in industry. It is mainly conditioned by the fact that the nanostructure is not kept during further sintering. However, with consideration of the general trend in production of very hard ultradisperse alloys with high strength and low wear there is large spectrum search underway for the optimal methods of fabricating WC and WC/Co nanopowders. And the addition of tantalum carbide and vanadium carbide and also VC–TaC solid solution prevent the grain growth during sintering [57].

Studies [58, 59] describe the process with application of mechano-chemical and plasma-chemical synthesis methods. Micro- and nanopowders of more complex composition of WC–35 % TiC–Co and Ti(C, N)–WC–Ni were obtained through carbo-thermal restoration and mixed grinding. Study [60] presents the research in which the nanopowders with the particle size less than 100 nm were not obtained, and the qualification of the powders by additives and fraction distribution were not fully completed.

Most big companies – H. C. Starck (Germany), Wolfram BHG (Austria), Dow Chemical Company (US) and others, specialized in production of hard alloyed WC powders, indicate the particle size less than 0.2…0.3 mkm in their product leaflets [61]. The US Company Inframat Corporation proposes WC and WC–(5…15 %) Co nanopowders with the sizes of carbide grains 40…70 nm, which, later on, can be agglomerated in particles with the average size 0.2…0.4 mkm [62]. The agglomeration process is conducted for preparation of the batch for compaction.

However, despite the numerous studies on the synthesis of nanocrystal refractory compounds mentioned above, it is difficult to compare the efficiencies of different methods for most cases, as a lot of important details for such a comparison (composition of additives, distribution of nanoparticles by size, response of

ultradisperse powders during compaction and sintering, properties of consolidated compacts, etc.) have not been studied yet.

The study into the fracture of nanostructural materials based on refractory compounds with the fractographic method has demonstrated the intercrystalline nature of their crack development. It has been found that fracture is running beyond the grain boundaries. The intercrystalline nature of fracture is explained by the fact that when the grain size decreases such an important characteristic of brittle materials as the fracture viscosity (crack resistance) does not virtually change for single-phase objects.

There is a lack of information about the high-temperature strength of nanostructural refractory compounds. Hardness is the most carefully studied characteristic of the nanomaterials based on refractory compounds and this can be explained by availability of the corresponding measuring equipment and relative ease of the sample preparation. The value of hardness is important during production of instrument materials. Even for carefully-prepared and well-qualified nanocrystal samples of titanium nitride and tungsten carbide the value of hardness exceeds that in conventional coarse crystalline analogies by 1.5...2 times and amounts to ~30 and ~40 GPa, respectively.

The prospects of research and development of nanomaterials based on refractory compounds are connected with the study into the nature of scale effects and the stability of nanostructures [63], and also with the revealing of new areas of application (in comparison with traditional instrumental and tribotechnical applications).

Study [64] emphasizes the possibility to use films based on molybdenum and tungsten carbides for electrocatalysis. Various distribution surfaces, the presence of non-equilibrium phases and boundary segregations in the structure, the presence of micro- and macrostresses, and potential porosity can cause deviation from equilibrium in nanomaterials and release excessive free energy.

However, what must be the optimal initial structure of nanomaterials (according to the operational conditions and economic reasons) cannot be analytically forecast and now this task is solved by means of empirical approaches.

3.2. Regular patterns of electroconsolidation for popular powders during hot pressing

Materials based on tungsten carbide are most frequently used due to their good wear resistance for drawing and cutting tools. These materials include in their composition the cobalt bonding connecting the WC grains and compacting the material

at comparatively low temperatures. However the cobalt bonding decreases the material hardness, the parameter that mostly determines the wear resistance of materials. Cutting inserts of pure WC have the wear resistance 8...10 times higher than that of inserts made of WC–Co used for cutting Steel Cr12M [65]. Products of pure WC powders are most frequently obtained with the methods of hot pressing and hot isostatic pressing. In this case the pressing temperature is 200...500 °C higher than the sintering temperature for the mixture of WC–Co powders, and, therefore materials with higher embrittlement can be produced. The impact viscosity can be increased by application of WC mixtures with tungsten, carbon, carbides and nitrides.

The most efficient methods for compacting materials heavy for sintering are the methods of compaction with application of heating with electric current, such as SPS and FAST. These methods are based on pulse electric current with an added external pressure (100 MPa), which can be sintered at various heating speeds. The sintering cycle is very short, naturally 1…5 min, which provides an insignificant grain growth. During sintering the electric current can initiate electric discharges in the zone of intraparticle contacts; these discharges provide formation of plasma causing clearance and activation of the surfaces of the powders sintered [66].

The clearance of particle surfaces of the powder results in formation of pure grain boundaries. For example, during the sintering of Al powders, which have on their surface a nonhomogeneous Al_2O_3 layer with the thickness of more than 5 nm, this layer is eliminated with an electric field, and the powder is compacted to the total density [67]. The electric field applied results in formation of the temperature gradient around the pores, which has a positive impact on compaction of large pores. At the intermediate stages when the area of different-sized pores is sintered, a charge gradient is formed. The electric resistance is increased when the concentration of equi-polar lines grows (fig. 3.1). The electric current density is maximal near the large pores. It creates a temperature gradient, thus the temperature is higher in the area of large pores.

The equation for calculation of the temperature gradient ΔT near a pore has the form [68]:

$$\nabla T \approx \frac{1}{R} \cdot \sqrt{\frac{\rho_0}{2 \cdot C_M} \cdot \frac{T_0 \cdot E_0^2 \cdot \Delta\tau}{n}}, \qquad (3.1)$$

where R – the pore radius, nm; ρ_0 – the electric conductivity, Ohm·m; C_M – the thermal conductivity; T_0 – the initial temperature, °C; E_0 – the stress capacity of the electric field; $\Delta\tau$ – the action time of the electric field; n – the number of electric impulses.

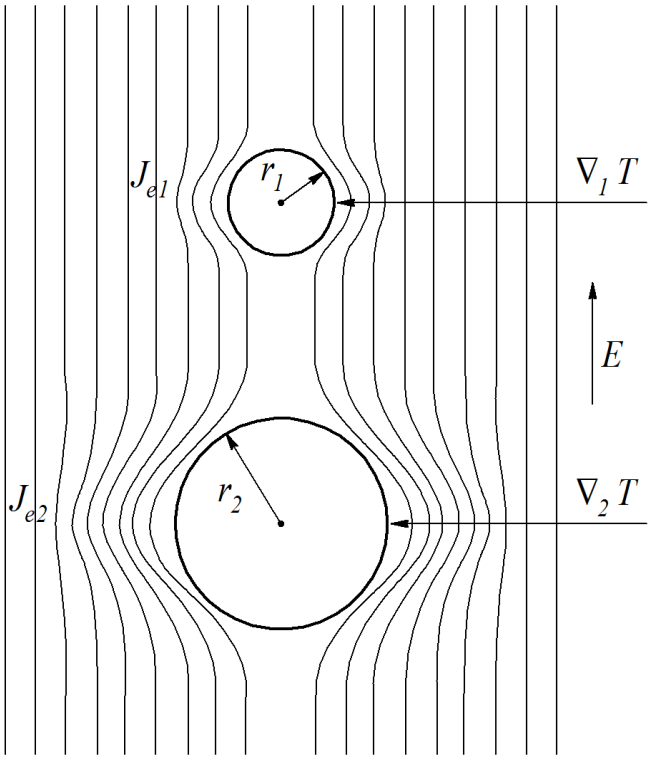

Figure 3.1 – Diagram of change in the electric field density near large and small pores [69]

The temperature gradient near a pore causes formation of the vacancy gradient ΔC_v. Yet more vacancies are formed near large pores. The vacancy flow J can be presented as follows:

$$J = D_v \cdot \left(\frac{K_T}{T} \cdot \Delta T - \Delta C_v \right), \tag{3.2}$$

where D_v – the vacancy diffusion coefficient; K_T – the thermal diffusion coefficient.

According to equation (3.2) the vacancies diffuse from large pores towards small ones, thus shortening the size of large pores. This process is opposite to the vacancy diffusion process under the conditions of conventional furnace sintering, when large pores grow at the expense of small ones.

During hot pressing under the conditions of heating with electric current (electroconsolidation) compaction goes over a short hold time, which prevents the grain growth. For example, a SnO_2 powder is sintered to the density 93 % at a temperature of 1163 K over 10 minutes. At the same time this powder during conventional furnace sintering is compacted at the temperature 1273 K over three hours only to the density 61 % [70].

During electric sintering of TiN nanopowder the total density is achieved at the temperature 1473 °C and the grain size is an order lower than that during the conventional sintering at 1673 K [71].

Without bonding during electrosintering there is the possibility to avoid cold pressing and distillation of the bonding. This stage takes up to 30 % of the production cost with the powder metallurgy method. Electroconsolidation can activate compaction and conduct sintering at much lower temperatures in comparison with those of hot isostatic pressing. The following high-density ceramics and metal materials were produced with electroconsolidation: $A1_2O_3$ and W [72]. The results obtained demonstrated high efficiency of the process with the application of electric current. High-density materials with the fine microstructure can be obtained at comparatively low temperatures and over short sintering time [73].

The following parameters were measured: density ρ_{rel}, hardness *HRA*, yield limit at bending σ_{bend}, grain size d_{mid} of the samples obtained at various *P* and *T*. The average values of measurements for three samples are given in table 3.1.

Table 3.1 – Some physical and mechanical characteristics of the samples obtained

Sample №	*P*, MPa	*T*, °C	ρ_{rel}	*HRA*	σ_{bend}, MPa	d_{mid}, mkm
1	45.0	1700	96.2	93	530	0.350
2	45.0	1730	99.0	95	720	0.420
3	45.0	1800	99.2	95	670	0.750

The data given in table 3.1 and the data of the electron microscopical study demonstrate that during high-temperature sintering under loading the grain size of WC has slightly increased, however it does not predominantly exceed 1 mkm. The materials are practically nonporous (fig. 3.2).

Thus, the values of σ_{bend} = 720 MPa obtained were high, though for WC obtained from the initial powders with the grain structure 2 mkm and 5 mkm by means of hot processing at T = 2500 °C, t = 10 min, P = 12 MPa, numerous literature sources give the value σ much lower, i.e. 350…520 MPa. The samples have the high values of fraction viscosity K_{1c} = 9.1 MPa·m$^{-1/2}$ at a high value of HRA, which plays an important role for cutting instrumental ceramics. During the hot pressing of tungsten monocarbide powders the pressure should be applied after the temperature 1000 °C, when the air from the pressing body has already come out, otherwise it may result in pore formation (fig. 3.3). Rapid hot heating, due to heterogeneous compaction in some parts of the sample, can lead to formation of large isolated pores.

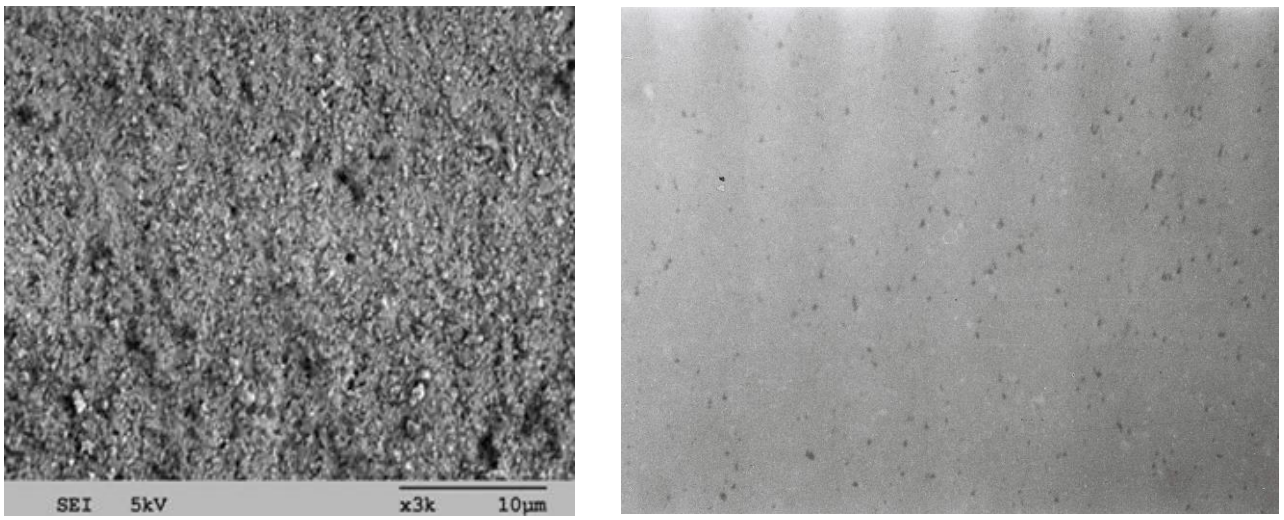

a *b*

Figure 3.2 – Fracture surface of the hot-pressed WC sample (*a*) and the structure (*b*) at T = 1700 °C and P = 45 MPa

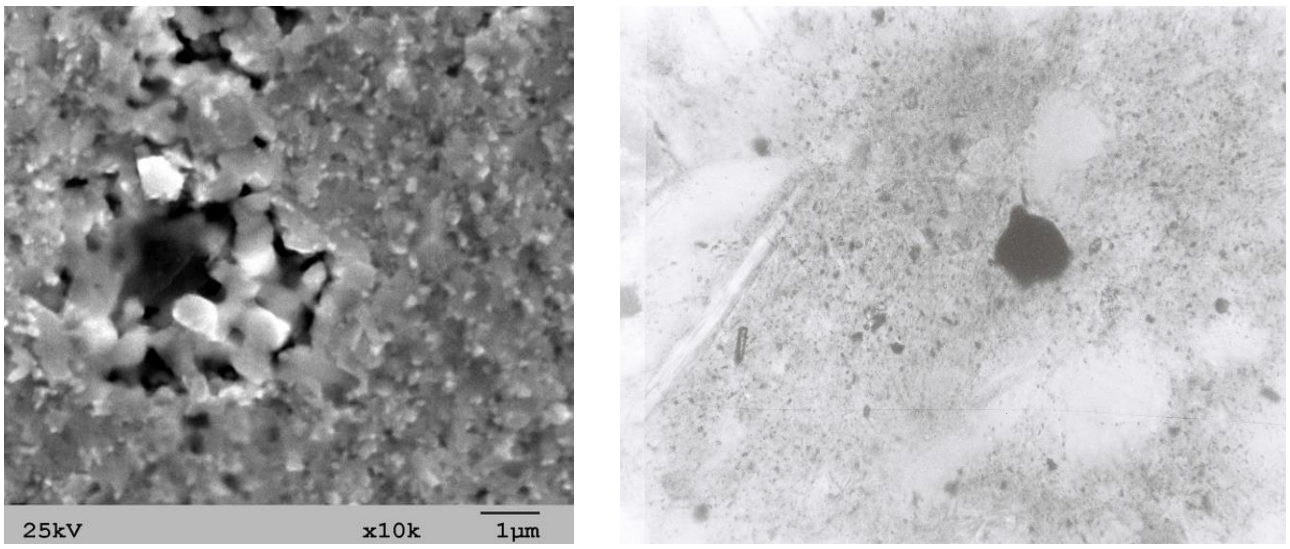

×20000 ×20000

a *b*

Figure 3.3 – Fracture of the structure (*a*) and the structure (*b*) of a tungsten monocarbide sample obtained at the temperature 1600 °C and the pressure 45 MPa

Therefore, the heating speed during hot pressing must be controlled: at the beginning the speed must be 50 °C/min till 300 °C, then it must be 250 °C/min till 900 °C, later on the isothermal hold must be conducted at 900 °C over 2…3 min and then the temperature must be increased at a speed of 500 °C/min till 1700 °C. In this case the residual CO gas can go out of the sample and later on the practically nonporous structure can be formed.

The highest probability of pore formation is high if the temperature rises at a speed of 500 °C/min. The higher fracture viscosity of the materials obtained from WC nanopowders is characterized, first of all, by highly dispersed grains and strong boundaries between them; it is conditioned by a short sintering time and formation of contact necks between the neighbouring grains.

The X-ray analysis showed that apart from the WC phase there were compounds of W_2C, $W_6C_{2.54}$. The X-ray of the WC samples is given in fig. 3.4.

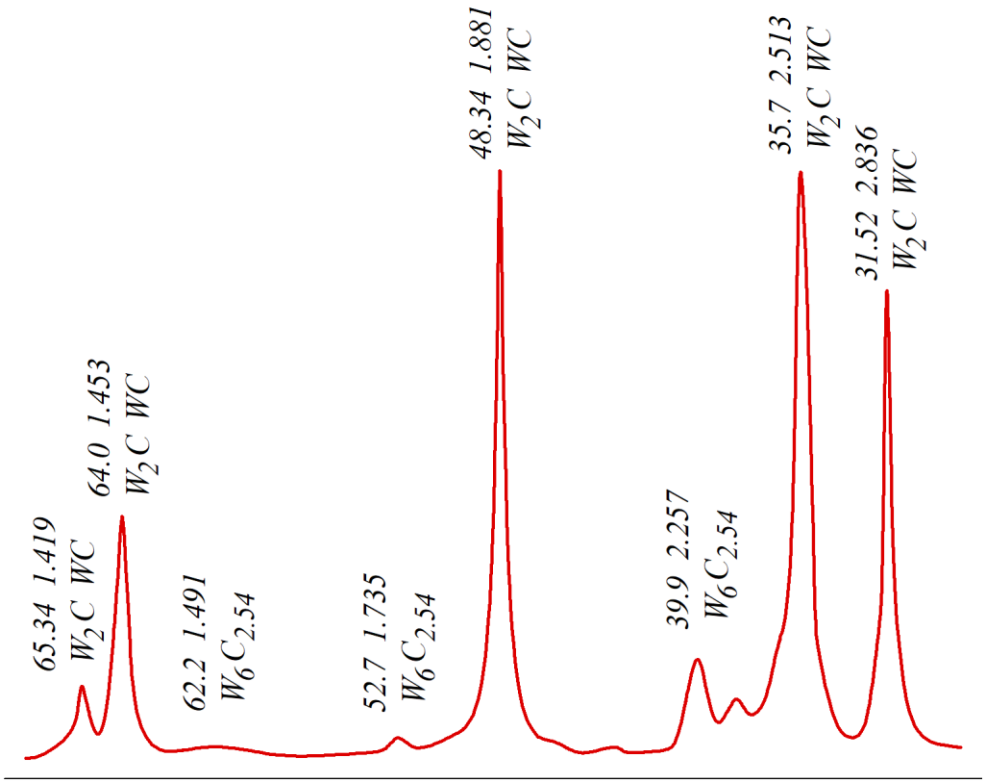

Figure 3.4 – X-ray of the tungsten monocarbide sample

Thus, the research conducted has demonstrated that the hot pressing method for nanopowders with DC heating accelerates the vacancy flow on the surfaces of pores, and a rapid decrease in porosity on the grain boundaries increases the boundary mobility and compaction due to grain packing through the sliding of grains on the boundaries.

3.3. Compaction mechanisms for tungsten monocarbide

Electroconsolidation is similar to conventional and activated sintering, hot pressing, and, on the level of elementary volume, micro-electric welding. However,

this method has some special features that advantageously distinguish it from other methods of powder consolidation. The regularities of the mechanism of sintering tungsten monocarbide nanopowders are not sufficiently studied. The earlier research has demonstrated that it is possible to fabricate the material with high physical and mechanical properties [74, 75]. It has been found that intensive mass transfer is conducted on the contact areas between the neighbouring particles under the impact of current. And rapid sintering is underway in the powder compacts.

According to the process parameters (pressure, current strength, voltage, heating speed, heating time) sintering can run by different patterns. And, therefore, the material structure and properties can vary in wide ranges. In conventional sintering the main driving shrinkage force is surface tension. Unlike conventional sintering, electroconsolidation due to the heterogeneous temperature field leads to heterogeneous vacancy distribution resulting in mass transfer. Besides, thermal diffusion also contributes to the mass transfer. The contribution of the surface tension and the forces from electric heating to mass transfer, and, thus, to a change in the pore sizes depends on the pore sizes. For the vacancy diffusion and mass transfer, in which the primary cause is surface torsion, the situation is opposite. Therefore, we can conclude that during electric sintering the number of large pores decreases at an accelerating rate.

It should be noted that large pores do not grow at the expense of small ones, which, as a rule, occurs during conventional sintering. In this case the sizes become smaller, and the number of small pores decreases. The total number of pores during electric sintering decreases less than that during conventional sintering. The quantitative regularities of a change in the size of a spherical pore after passing the current through the environment without the external pressure are given in [76]. The temperature of the powder is higher near the pore surface, therefore the temperature gradient during heating activates the vacancy flow to the pores, and thus it results in the pore growth. At the same time the increased vacancy concentration near the pore surface results in formation of the vacancy flow from this surface, thus the pore shortage. It can be assumed that a pore will further annihilate when it is away from the powder surface. This can be caused by heterogeneous vacancy concentration, which corresponds to high temperature; meanwhile on the pore surface such concentration is set virtually instantly.

In the vacuum chamber (fig. 3.5) tungsten monocarbide was sintered to the density 99 %. Nanodisperse powder obtained with the plasma-chemical method was used as the initial powder.

The sintering process was accompanied by some events recorded with different devices and tools. The observation over these phenomena and their change when the

technological parameters have changed can control the sintering process and direct it as needed for fabricating the materials with the given properties in order to produce the given forms and sizes.

Figure 3.5 – Vacuum-sintering chamber

Refractory super-hard substances, particularly, tungsten carbide, are solid and brittle. During sintering the workpiece shrinkage can reach 60% according to the initial density. This shrinkage goes along with a decrease in the number of defects in the crystal structure, roughness of the particle surface, porosity, and also an increase of grain growth and homogenization of alloys. The following two phenomena are directly connected with sintering: increase of the contact surface between the particles and the closeness of the particle centers (shrinkage), the other mentioned phenomena are just accompanying. As known, the sintering process approaches the system consisting of individual particles to the thermal dynamic equilibrium, thus it is the process during which excess energy of the system decreases. During homogeneous pressing only the excess energy of the free boundary surface and defects of the crystal mesh can be expressed. This energy is the main driving sintering force. The value of this driving force can be assessed with consideration of the sizes of the particles that form the workpiece. For example, the specific surface of carbide powders after grinding, as a rule, amounts to 1…5 m^2/g; and for the powders obtained with plasma-chemical synthesis this value is 10…40 m^2/g.

If we assume that any formation method can produce workpieces with the porosity 40 %, we can calculate the excess energy of this system. The free surface energy in the pressing volume is rather high. It is this energy that performs the main work of compaction during which the substance flows to the cavity (pores). With some

approximation we can assume that the substance flows to the surface with negative curvature under some effective pressure from the surface torsion:

$$P_{e.s.} = \frac{2 \cdot \gamma}{r}, \tag{3.3}$$

where γ – the free surface energy, mJ/mkm^2; r – the grain size, mkm.

This pressure is rather high for pressing the disperse particles, where the pore size can be compared with the particle size. The equivalent pressure, at least in the initial period of sintering, for disperse powders is very high, and, naturally, causes a rapid compaction due to the creep mechanism:

$$\varepsilon = A \cdot P_{e.s.}^{\nu} \cdot \exp\left(\frac{-E_{c.a.}}{R \cdot T}\right), \tag{3.4}$$

where A – the creep coefficient; ν – the constant; $E_{c.a.}$ – the creep activation energy, kJ; R – the gas constant; T – the sintering temperature, °C.

The other driving force of compaction together with the excess energy is the energy of the grain boundary distribution, which divides the crystalline areas with various orientations one from another.

It should be noted that during heating, at first, the physical contact is formed between the particles in a compact, later on – the developed boundary system; thus at the beginning the free surface energy, which causes compaction of the system, is also spent on formation of boundaries the excess energy of which will be the driving force of sintering.

Formation of the developed boundary system is the result of thermally activated sliding along the grain boundaries at the initial stage of sintering.

Therefore, during slow heating to the sintering temperature, the perfect flat boundaries of a short length are formed, and compaction goes very slowly, which leads to grain growth. And, on the contrary, due to a rapid heating according to the mechanism of thermally activated sliding beyond the nanograin boundaries and due to the fact that the boundary division surface is one order less than the nanopowder surface, further compaction of the compacts goes according to the similar creep mechanism as described in (3.4), but much faster:

$$\varepsilon' = A_1 \cdot P_{e.b.}^{\nu} \cdot \exp\left(\frac{-E_{c.a.}}{R \cdot T}\right), \tag{3.5}$$

where $P_{e.b.}$ – the effective pressure, Pa, conditioned by a shortage of the boundary division surface, $P_{e.b.} \prec\prec P_{e.s.}$.

The following driving force of sintering is the energy of imperfections in the crystalline lattice. It is the reason of accelerated exchange of the sites:

$$n_a = n_0 \cdot \exp\left(\frac{-E_{a.an.}}{R \cdot T}\right), \tag{3.6}$$

where n_a – the number of atoms departing their places in the lattice and occupying the vacancy unit; n_0 – the structural factor not depending on the temperature; $E_{a.an.}$ – the activation energy of defect annihilation, kJ.

This value in the distorted lattice is decreased considerably. Therefore active compaction requires strong breakdown of the structure through grinding the substance; this process goes in the powders obtained with the plasma-chemical method. During sintering the number of imperfections in the crystal lattice is considerably decreasing. For example, in tungsten monocarbide with the specific surface up to 1 m^2/g the size of coherent areas is 20000…50000 nm, and after sintering at the temperature $0{,}8 \cdot T_{mel}$ it becomes 200000…500000 nm.

During elecrononsolidation in the moment when the current passes through the areas of interparticle contacts there occurs high electric resistance leading (over a very short time of approximately 1…2 seconds) to an increase in the temperature more than 3000 °C, which results in activation of the surfaces of the sintered powders at the expense of evaporation. Greater closeness of the particles centers, i.e. pressing compaction, is the result of external mechanical pressure with the simultaneous action of electric current.

The time of action of high temperature in the interparticle distance cannot be determined accurately, however, we can assume that the plasma column due to the impact of the own magnetic field is similar to that described in [77], and may succumb to rapid deformation and destruction.

Fig. 3.6 gives an expected diagram according to which DC or AC current goes through the particles of conducting tungsten monocarbide.

The voltage difference applied to the powder causes a rapid rise in the current. When current begins to go, the boundaries of layers with higher electric conductivity move from the sample's surfaces contacting with the end parts of the electrode-punches depthward this sample. The value of current increases abruptly when both these layers join in the central part of the sample. The growth rate of these layers with higher electric conductivity is in direct ratio to the electric voltage and pressure to the powder.

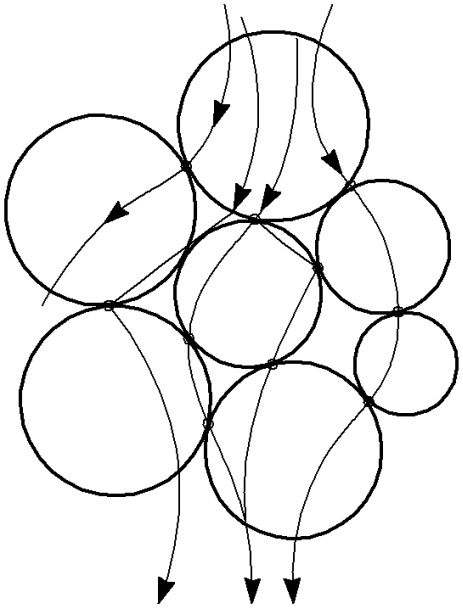

Figure 3.6 – Diagram of electric current going through WC powder

The electric energy turns into the thermal energy on the contact resistances of the areas where the powder particles contact, on the contact resistances of the electrodes/punches/powder dividing surfaces, and on the electrodes/punches resistances. Fig. 3.7 demonstrates the compaction process of tungsten monocarbide nanopowders with the initial grain size 70…90 nm.

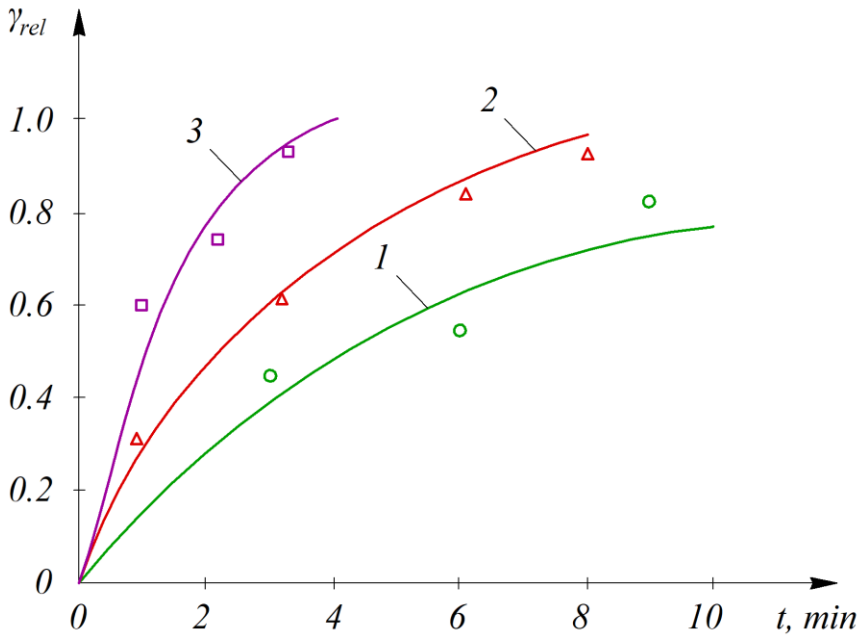

Figure 3.7 – Change of the relative density of tungsten monocarbide nanopowders:
○ – 50 °C/min; Δ – 250 °C/min; □ – 500 °C/min
(pressure rises slowly from 10 MPa at 400 °C and from 45 MPa at 1650 °C)

The shrinkage change depends on the temperature and the rate of temperature growth; this dependency is demonstrated in fig. 3.8. A considerable shrinkage during hot pressing begins from 800…900 °C. During sintering the pressure slowly rises from the moment when the intensive shrinkage starts. The residual pressure is applied at the temperature 1400 °C when the shrinkage speed falls considerably. At 1550…1600 °C the shrinkage virtually stops.

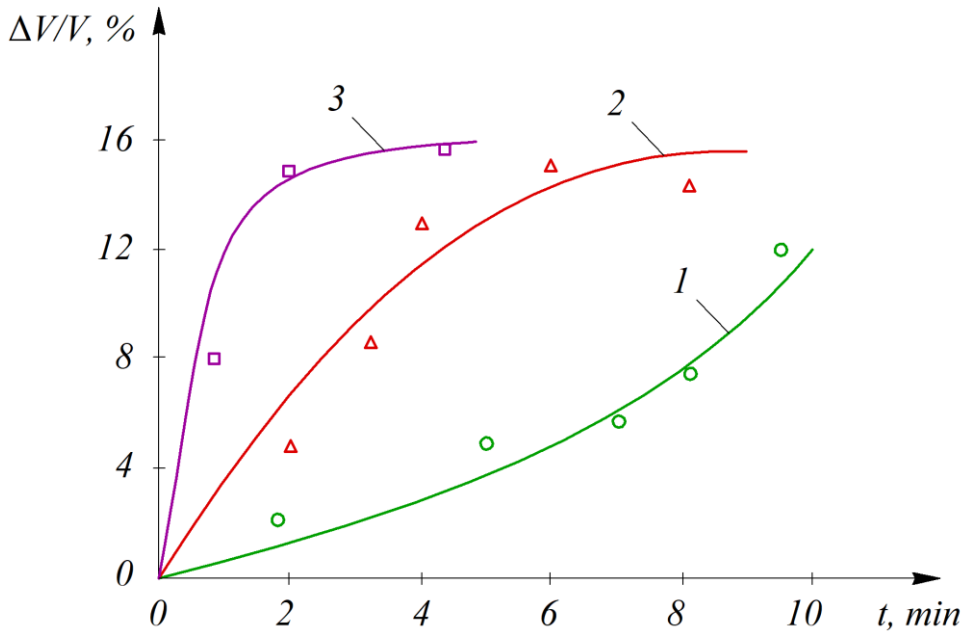

Figure 3.8 – Dependency of shrinkage on the heating rate at T = 1700 °C, P = 45 MPa:
○ – 50 °C/min; Δ – 250 °C/min; □ – 500 °C/min

The process of hot pressing is comparatively insensitive to the composition of powder particles, their form and distribution by size.

Unlike electroconsolidation, especially its initial stage, due to the important role of interparticle contact resistances, nanodisperse particles have high resistance due to a great amount of contact areas.

The amount of thermal emission on the interparticle contacts increases when the size of particles decreases.

As far as the specific capacity is the product of the powder resistance and the squared current strength, and the current is determined not only by the resistance level of the powder, there is no correlation between the particle sizes and the capacity consumed.

Fig. 3.9 gives the dependencies of the current capacity on the secondary coil on the sintering temperature.

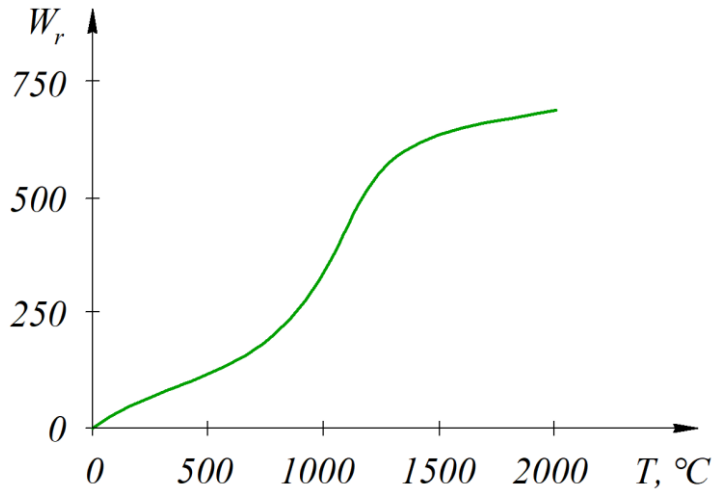

Figure 3.9 – Dependency of the net capacity consumption W_r for sintering tungsten monocarbide on temperature (W_r – the product of electric capacity and the number of AC cycles at the frequency 50 Hz)

The process of compaction during sintering with electric current can be described by the equations of hot pressing or sintering under pressure:

$$\frac{d\Theta}{dT} = \frac{k \cdot e^{\left(-Q - \frac{5}{3} \cdot \frac{Q'}{R \cdot T} \cdot\right)}}{H^{-2/3}}, \tag{3.7}$$

where Θ – the porosity; Q, Q' – the activation energy of shrinkage and grain growth, respectively, kJ; H – the heating speed, °C/min.

As seen from equation (3.7) the speed of compaction of tungsten monocarbide is proportional to the heating speed. Here the powder compaction level m was taken equal to 5, and the grain growth level n = 3.

As mentioned above, higher closeness of the particles centers (e.g., pressing compaction) is the result of external mechanical pressure with the simultaneous action of electric current.

This equation is based on an insignificant impact of the capillary (Laplace) pressure and the dissipation energy during sintering and compaction. However the formula given above does not include the friction on the press mold walls, the height and the diameter of the press mold.

The contact neck growth of grains is controlled by the surface grain self-diffusion.

The volume shrinkage has the following approximate dependency on the contact neck radius:

$$\frac{\Delta V}{V} = 3 \cdot \frac{\Delta R}{R}. \tag{3.8}$$

Expression (3.8) does not include the particle re-grouping.

It is assumed that each rotation results eventually in higher density as soon as large pores are filled with particles, small intragrain pores disappear at the expense of reduction of the intragrain distances. It is assumed that each rotation act of particles at the angle $\varphi = 1$ decreases the total volume in the size R^3, which can restrict the particle rotation with the coordination number n less than 4 and, in this case, the shrinkage equation can have the form [78]:

$$-\frac{d}{dt}\left(\frac{\Delta V}{V}\right) = \frac{A_r \cdot g_4 \cdot D_b \cdot \sigma \cdot \Omega \cdot R}{k \cdot T \cdot x^4}, \tag{3.9}$$

where g_4 – the static weight of the particles compacted randomly, if the coordination number is less than 4; A_r – the numerical constant equaling 0.1; D_b – the coefficient of surface self-diffusion; R – the radius of particles, nm; x – the neck size, nm.

The value g_4 depends on the average value of the relative density. It should be noted that powder particles, while the current is passed, are subject to reduction by the electro-magnetic forces.

If the current is uniformly distributed (with equal density) across the section of the cylindrical powder column with the radius r_0, the pressure $p(r)$, Pa, can be determined by the formula:

$$p(r) = \frac{-\mu_0 \cdot \left(r_0^2 - r^2\right) \cdot I^2}{4 \cdot \pi^2 \cdot r_0^4}, \tag{3.10}$$

where μ_0 – the magnetic constant, $\mu_0 = 1.256 \cdot 10^{-6}$ g/m; r – the radial coordinate, m; I – the current force, A.

The distribution of pressure is similar to that described in [79] for metal powders. The diagram of this phenomenon is given in fig. 3.10.

Fig. 3.11 demonstrates that an increase in the capacity on the secondary winding amplifies the mechanical properties of tungsten monocarbide, because a rise in the capacity increases the sintering temperature.

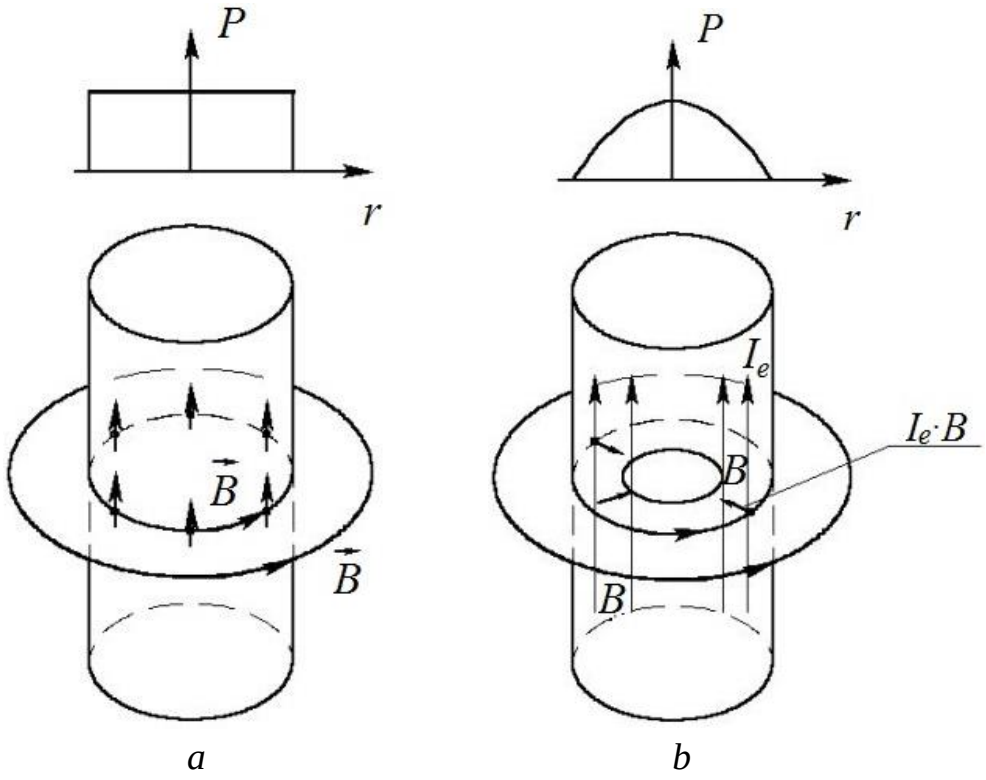

Figure 3.10 – Pinch effect in the powder being sintered and the pressure distribution: *a* – homogeneous distribution of the current *I* in the powder column (induction *B* has the azimuth direction, $\vec{B}$ – the radial direction to the conductor axis); *b* – conductor with the surface current (I_e – the current density constant, $I_e = I/s$, *s* – the cross section square)

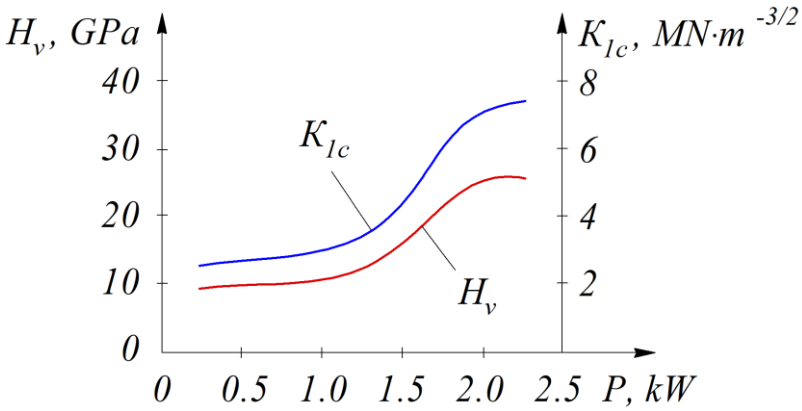

Figure 3.11 – Change of the micro-hardness and the fracture viscosity according to the current capacity

Table 3.2 gives the comparative properties of the samples of submicron and nanopowders (0.5 mkm), WC nanopowders (40…70 nm), and standard VK8 hard alloy.

Table 3.2 – Comparative properties of the samples out of submicron and nanopowders (0.5 mkm), WC nanopowders (40…70 nm), and standard VK8 hard alloy

WC samples	1	2	3	WC nano	VK8
Sintering temperature, °C	1630	1750	1800	1740	1450
Hold time, min	1	20	20	1	60
Relative density, %	98.7	99.1	99.8	99.2	99,0
Average grain size, mkm	0.5	2.1	5.5	0.1	3…4
Vickers hardness HV_{10}, GPa	24.3	20.3	18.4	26.4	16
Fracture viscosity, MPa·m$^{1/2}$	9.1	8.2	7.6	10.9	12

Table 3.2 demonstrates that the hardness and the fracture viscosity of the samples obtained from tungsten monocarbide nanopowders are significantly higher than those in the submicron powder samples.

Additives of chromium and vanadium carbides (table 3.3) can slightly increase the hardness and do not virtually impact the fracture viscosity. The relative density also decreases; it may be the result of lower activity of the grain-boundary creep during hot pressing.

Table 3.3 – Properties of the samples obtained from WC nanopowders (40…70 mkm) with chromium and vanadium carbide additives

WC samples	WC nano	2 vol. % Cr_2C_3	2 vol. % VC
Sintering temperature, °C	1640	1640	1640
Hold time, min	2	2	2
Relative density, %	98.9	98.6	98.6
Average grain size, mkm	0.1	0.35	0.35
Vickers hardness HV_{10}, GPa	24.4	24.6	24.7
Fracture viscosity, MPa·m$^{1/2}$	9.2	9.8	9.7

Thus, even a slight amount of carbide additives of such refractories as chromium and vanadium triggers the grain growth. Obviously, this can be explained by the fact that these additives activate diffusion processes during hot pressing, which gradually encourages the grain growth.

CHAPTER 4

RESEARCH INTO THE OPERATIONAL PROPERTIES OF THE MATERIALS OBTAINED

4.1. Research into the physical and mechanical properties of the materials obtained

The research into the physical and mechanical properties of the samples with the fine structure has demonstrated that such mechanical characteristics as strength, hardness, and fracture viscosity are higher than those of products with the rough structure. Fig. 4.1, *a*, *b*, *c*, and *d* present the comparative characteristics of different refractory compounds with materials obtained of tungsten monocarbide and alumina nanopowders.

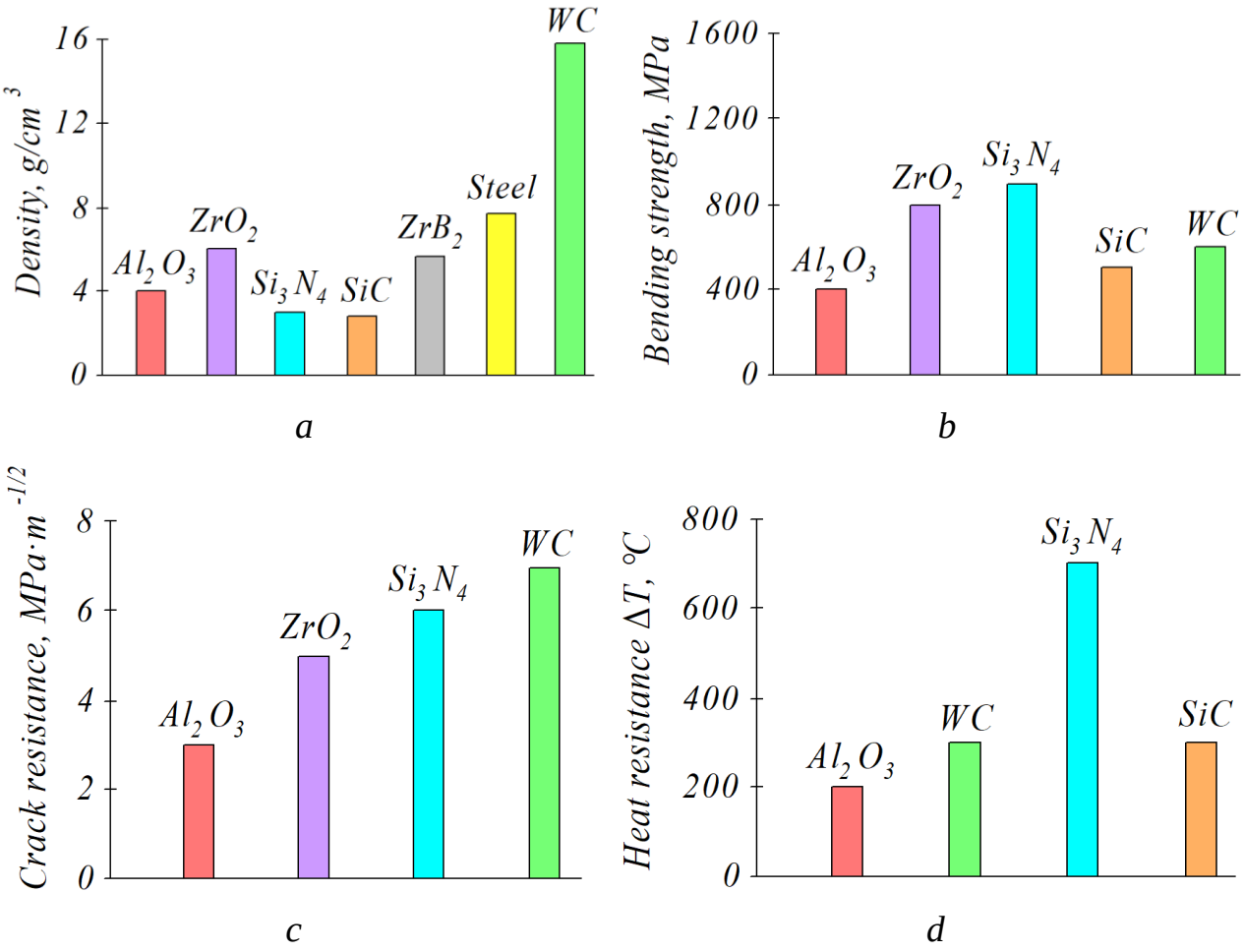

Figure 4.1 – Some comparative property of the materials (Al_2O_3, WC obtained out of nanopowders)

The given diagrams (fig. 4.1) demonstrate that the mechanical properties of the materials based on tungsten monocarbide and alumina with the fine structure are better than those of the materials with rougher structure, meanwhile a change in the physical properties is less visible, with the only exception of the high-temperature strength of tungsten monocarbide, which is much higher in comparison with that of tungsten monocarbide with the rougher structure. It can be explained by a considerable rise of the thermal conductivity of this material due to its fine-grain structure and strength of intragrain boundaries.

The comparative characteristics of the cutting properties of different instrumental materials based on finely dispersed tungsten monocarbide can demonstrate that these materials have their own application field where they are implemented most efficiently. Fig. 4.2 demonstrates their potentially efficient field of application.

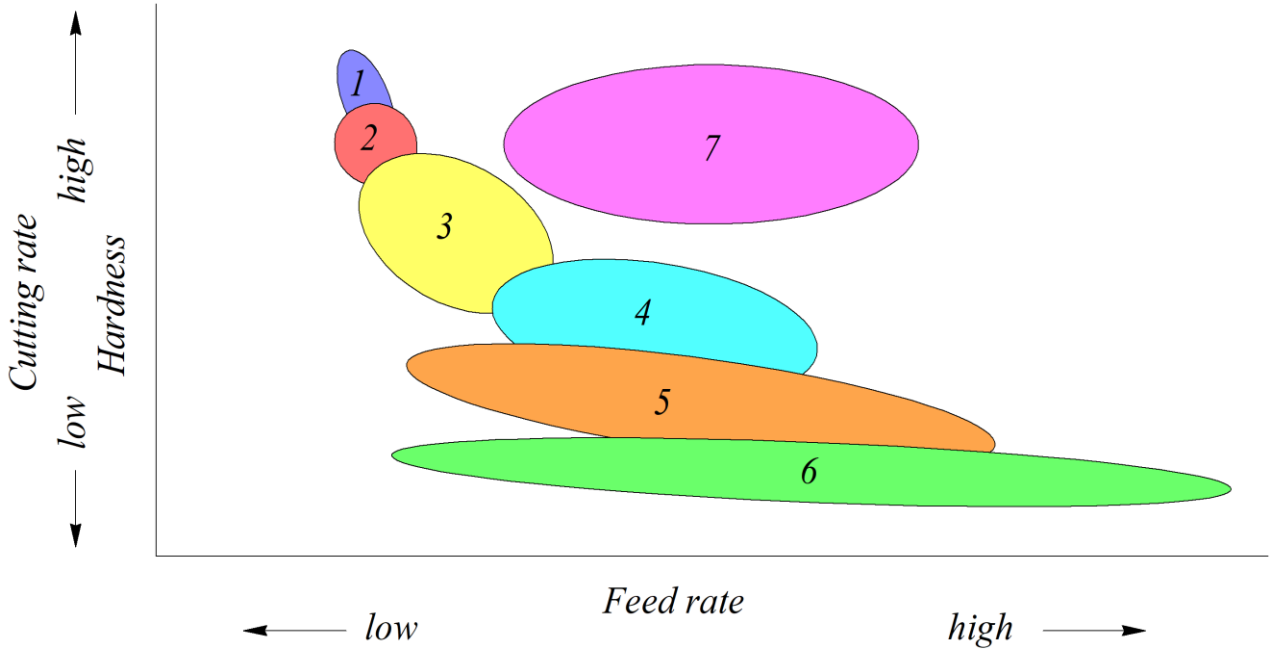

Figure 4.2 – Fields of application for various instrumental materials:
1 – PCBN, PCD; *2* – ceramic; *3* – cermet; *4* – coated hard alloy;
5 – hard allow without coating; *6* – ultra fine-grain alloy;
7 – WC without bonding

Fig. 4.2 demonstrates that unlike fine-grain hard alloys the material based on tungsten monocarbide can work at much higher cutting speeds, and, therefore, it successfully competes with ceramics of cubic boron nitride and, due to its higher strength, can work at rough feeds and with higher cutting depth; thus, the prospects of application of this material are good.

4.2. Research into the cutting properties of tungsten monocarbide inserts

Refractory materials of the groups “tungsten carbide – cobalt” and “tungsten carbide – titanium carbide – cobalt” are instrumental materials applied in metal processing at present. Cobalt is the most frequently used bonding that provides the required strength and can be used to fabricate materials at comparatively low sintering temperatures due to formation of the liquid phase. At high processing speeds the temperature in the cutting zone can reach 800...1000 °C, and under these conditions the hardness of an instrumental material falls abruptly due to the presence of cobalt; this results in a rapid decrease in the wear resistance.

As far as at present production and engineering are increasingly using alloys and materials that have poor processability, the issue of better workability and durability of these materials are of importance. For example, the processing of hardened steel with great amount of nickel at the speed 150 m/min increases the temperature up to 1000 °C. At this temperature the physical and chemical processes of interaction between instrumental and process materials, especially diffusion processes, are activated. The distribution of wearing mechanisms while processing Steel 12Cr18N10 is given in fig. 4.3 [80]. The testing made during the processing with cutting inserts of the developed instrumental material based on tungsten monocarbide without bonding has demonstrated that the distribution of wearing mechanisms is similar, however, as far as the material is rather hard, the factor of abrasive wear decreases.

It should be noted that in both cases the testing was conducted without cooling lubricants, which considerably intensified the impact of diffusion and oxide wearing. The application of cooling lubricants can decease the temperature in the cutting zone and slow down the diffusion and oxide wearing.

During the processing of comparatively brittle alloys, which are similar to cast iron, the segmental chip is formed and this causes high alternating loads in the instrumental material. Normally, this causes tool breakage. Here, the cobalt bonding can increase the strength of the instrumental material at relatively low cutting speeds. At high-speed processing the bonding does not provide the needed strength and hardness of the instrumental material.

Titanium alloys have high strength and viscosity. The reinforced titanium chip during cutting creates a wear crater on the frontal surface of the tool, which eventually causes its breakage. During processing with hard-alloyed plates the cobalt bonding creates an additional source to decrease the hardness.

The instrumental material based on tungsten monocarbide nanopowders has high hardness. Despite its strength this alloy is inferior to traditional ones, but at small

alternative loads it can be used not only as cutting material but also as the material for sandblasting and water-jet nozzles requiring high abrasive strength.

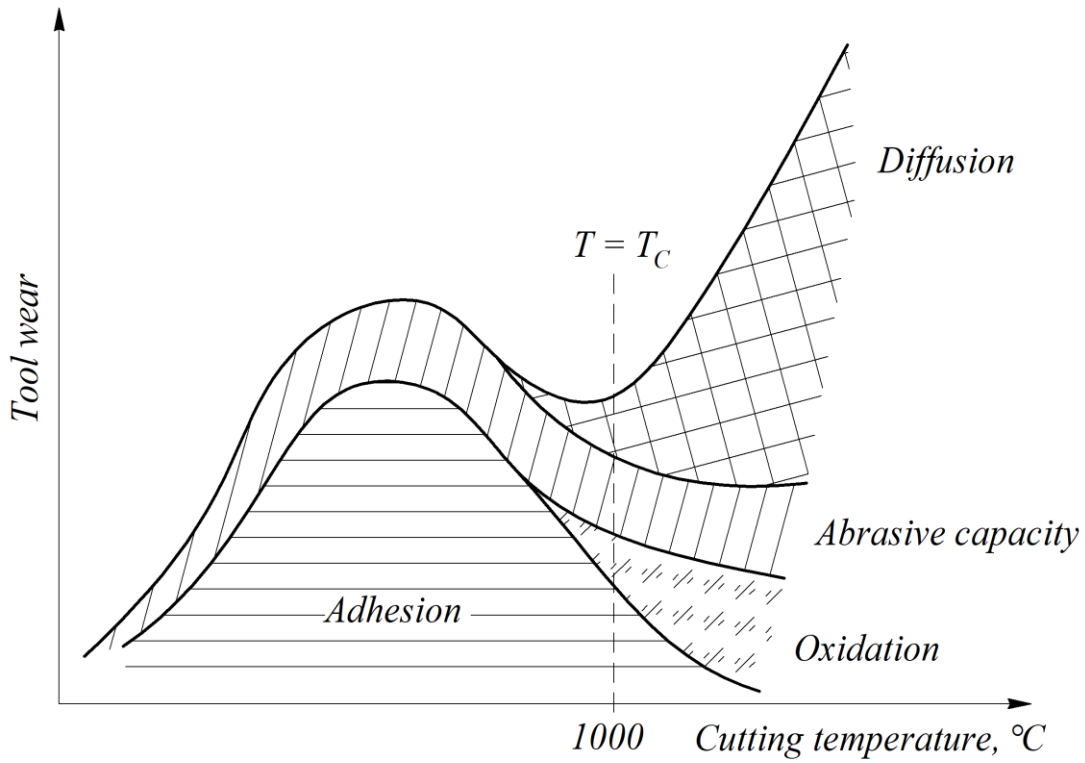

Figure 4.3 – Wearing mechanisms of the material based on tungsten monocarbide during the processing of Steel 12Cr18N10 with the hardness HRC 56…58

As known [81] the formation stage with the further distillation of the bonding takes up to 30 % of the production cost for the goods manufactured with the powder metallurgy method. If tools are produced of tungsten monocarbide nanopowders, there is no need to use special compound materials during the technological production process of such instrumental material. Such an important technological operation as the mixing of powders is also excluded. The possibility to sinter nanopowders with electric current without sintering additives considerably shortens the technological cycle for producing inserts and prevents formation of additional sources for cracks and pores. A rapid rise in the temperature during hot pressing restricts the grain growth. Table 4.1 gives the comparative characteristics of cutting inserts.

In this case Steel Cr12M (HRC 52...55) was processed at a cutting speed of 200 m/min, a feed of 0.1 mm/revs and a cutting depth of 0.2 mm.

Table 4.1 demonstrates that the relative density of the material based on nanopowders is lower than that of the material with the micron grain size. In this case the relative density does not characterize the actual porosity. The crack resistance is slightly inferior to that of the metal with cobalt bonding.

Table 4.1 – Some characteristics of cutting inserts

Characteristic	Developed instrumental material based on tungsten monocarbide nanopowder	VK6
Maximum sintering temperature, °C	1540	1450
Hold time, min	1	60
Relative density, %	97	99
Average grain size, mkm	0.3	3…4
Vickers hardness HV_{10}, GPa	4	16
Crack resistance, MPa $m^{-1/2}$	10	9…12

Table 4.2 presents some data on different cutting inserts during processing Steel 18CrMnT with HRC 52…55.

Table 4.2 – Strength of different cutting materials in processing Steel 18CrMnT

Cutting speed, mm/min	100	100	100	300	300	300
Feed, mm/rev	0.1	0.5	1.0	0.1	0.5	1.0
Cutting depth, mm	0.5	2.0	4.0	0.5	2.0	4.0
Strength VK8, min	12	8	5	8	6	3
Strength of the developed instrumental material based on tungsten monocarbide, min	30	28	20	25	22	10
Strength of oxide-carbide ceramic VOC71, min	21	15	8	10	8	5
Strength of Hexanit-P, min	34	29	22	27	23	11

The designed instrumental material based on tungsten monocarbide has high wear resistance and is promising for application as a cutting material for processing high solid steels and alloys as well as sand-blasting and water-jet nozzles. Application of this instrumental material can abruptly increase the efficiency at higher processing speeds and considerably increase the operational life, and, in some cases, replace an expensive tool of cubic boron nitride.

The processing with plates of the designed instrumental material based on tungsten monocarbide even for such refractory material as Ferro-Titanit S, the strength of which is slightly inferior to that of the cubic boron nitride. The process material is a material fabricated with powder metallurgy methods. Generally, it is the mixture of TiC (45 vol.%) and Fe (55 vol.%).

The steel matrix includes ferrite-pearlite or nickel-martensitic grains. Ferro-Titanit S is used as an instrumental material, and for production of different wear resistant details.

The hardness of Ferro-Titanit S is HRC 69 and its density is 6.5 g/cm^3. The fabrication of Ferro-Titanit S with powder metallurgy methods can prevent formation of the fiber textured structure and segregation, thus providing high density, strength and hardness. The material is easy in high-temperature tempering and has low thermal expansion. Due to these characteristics it is widely used in automobile and aircraft industries.

Abrasive grains of titanium carbide embedded in its steel matrix structure considerably complicate the processing with conventional blade tools due to the high-speed abrasive wear. And comparative testing of different instrumental materials was made for replacement of traditional widely used tools of cubic boron nitride. The material described above was processed in advance with hard-alloyed inserts with the wear resistant coating produced by “Sandvik Coromant” (Sweden) and the inserts of cubic boron nitride Hexanit R; the following cutting modes were used: cutting speed – 8 m/min, feed – 0.05…0.1 mm/revs, and cutting depth – 1 mm.

The instrumental material based on tungsten monocarbide has demonstrated high hardness and wear resistance in comparison with instrumental materials based on cubic boron nitride.

The comparative testing was made for different instrument materials. The results of this testing are given in fig. 4.4.

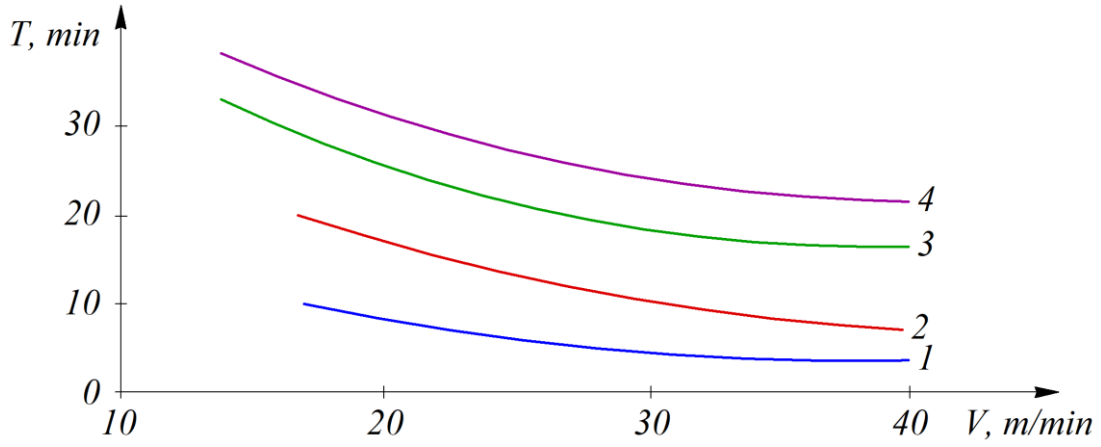

Figure 4.4 – Dependency of the strength of instrumental materials on the cutting speed during the processing of Ferro-Titanit S:
1 – insert T5K10; *2* – hard-alloyed insert with the coating produced by “Sandvik Coromant” (Sweden); *3* – designed instrumental material based on tungsten monocarbide; *4* – BN “Valenite” (US)

Ferro-Titanit S was processed with boron nitride inserts at speeds of 10, 20 and 40 m/min, a feed of 0.1 m/min, and a cutting depth of 0.2 mm. The testing was conducted on a 16K20 screw-cutting lathe. The workpiece of Ferro-Titanit S was fixed on one side in the bench holder and pressed with the poppet head center on the other side. The maximum wear intensity of the inserts on the back surface was observed at a turning speed of 40 m/min, the maximum strength at 10 m/min – 25...26 min for one cutting edge. The wear on the back surface equaling 0.4 mm was taken as the wear criterion. Inserts with a front angle of –5° and a back angle of 5° were used. For turning with the tools based on hard alloys the feed and the cutting depth were constant: 0.1 mm/rev and 1 mm, respectively. The cutting speed was taken equal to 10 and 20 m/min. The processing with hard-alloyed disposable inserts with the coating produced by "Sandvik Coromant" (Sweden) is accompanied by intensive wear on the coating surface due to strong abrasive action of the process material especially at high cutting speeds. Fig. 4.5 demonstrates the wear pattern of the cutting inserts.

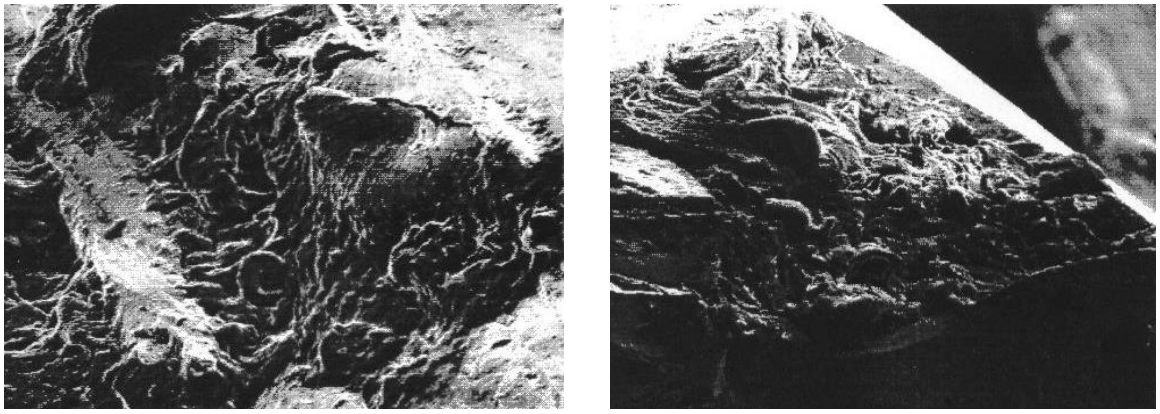

a *b*

Figure 4.5 – Wear pattern on the back surface of the inserts based on:
a – boron nitride (Valenite, US); *b* – designed instrumental material
based on tungsten monocarbide (Ukraine)

In the research for a speed of 10 m/min, the strength of the cutting edge of the hard alloyed insert produced by "Sandvik Coromant" amounted to 10...12 min, the new designed instrumental material based on tungsten monocarbide at the same cutting modes demonstrated the value almost three times longer.

The wear of the inserts based on tungsten monocarbide was also abrasive (fig. 4.5, *b*), however, at cutting speeds of 40 m/min and higher a small built-up edge periodically appeared, which disappeared under application of cooling lubricants. It should be noted that if cooling lubricants were used the strength of conventional hard

alloyed inserts increased from 20 to 40 %. Application of cooling lubricants can prevent formation of a built-up edge, but in this case there appears an evident wear crater, which, eventually results in cutting edge scaling during formation of a worn area over 0.8 mm on the back surface. The wear of the inserts based on the designed instrumental material of tungsten monocarbide (Ukraine) and of cubic boron nitride manufactured by Valenite (US) is predominantly abrasive. At cutting speeds of 40 m/min and higher the wear of the inserts of tungsten monocarbide is abrasive-diffusive. This explains the formation of a small wear crater on the front surface separated by the non-worn area from the cutting edge. The section of the wear crater in this insert testifies the absence of plastic shearing deformation of the material.

As known, the diffusive wear speed depends on the speed at which the atoms diffuse from the tool to the workpiece material. Despite the fact that carbon atoms are small and can rapidly travel between the iron atoms, in the cutting insert material they are closely connected with tungsten and cannot move independently. Regular wear of carbide grains confirms the possibility of diffusive wear. As far as the cutting insert based on tungsten monocarbide has no cobalt, the wear on the back surface is much slower than that in T15K6 inserts.

The research into influence of the form and sizes of the inserts under study demonstrated that the stability period according to the allowable wear criterion for different inserts has the similar dependency on the cutting depth. The feed from 0.05 to 0.1 mm/rev practically does not affect the wear in the inserts under study. However, the feed values over 0.1 mm/rev change the chip separation pattern. Particularly, during processing with the inserts based on tungsten monocarbide the length of discontinuous chip increases with simultaneous sticking of its fragments, thus resembling continuous chip. It may be explained by the lower friction coefficient between the front surface of the tool and the process material. This effect was not observed for the other instrumental materials under study, even if cooling lubricants were used.

Thus, the testing has demonstrated that the new instrumental material based on tungsten monocarbide is characterized by high wear resistance and is promising for processing refractory materials, particularly Ferro-Titanit S. Application of this instrumental material can increase the processing efficiency several times in comparison with that of hard alloyed materials traditionally used.

The range of application of the material designed can be expanded by means of different additives of alumina nanopowders, and the research into its improvement was also made.

The best cutting properties were demonstrated by the composition with 50 % vol of both components. The cutting properties of this and other instrumental materials for

processing Steel U8 with the hardness HRC 54...56 are given in table 4.3. The wear on the back surface equaling 0.4 mm was taken as the wear criterion.

Table 4.3 – Comparative wear resistance of some instrumental materials used for processing Steel C8 with HRC 54…56

Material of the cutting edge	Cutting speed, m/min	Feed, mm/rev	Depth, mm	Strength, min
VOK71	80	0.075	0.5	80
WC–50 mass% Al_2O_3	80	0.075	0.5	85
VK6	80	0.3	0.5	50

Table 4.3 demonstrates that cutting inserts obtained from the mixture of alumina (50 mass %) and tungsten carbide (50 mass %) nanopowders have higher wear resistance than ones of oxide-carbide ceramic with additives of the VOK71 zirconium oxide. It is explained by high hardness and strength of the material, which is the result of its fine structure and strength between the grains.

4.3. Research into the composite material for abrasive waterjet

Waterjet cutting is fulfilled with a liquid flow formed appropriately that is going out of the special nozzle with the diameter 0.08…0.5 mm at the supersonic speed (1000 m/s and more) and that provides the working pressure 400 MPa and more to the workpiece. As far as the distance from the nozzle edge to the material surface is several millimeters, the jet pressure exceeds the strength limit of the material; these are the conditions for cutting.

There are two methods of waterjet cutting for materials: waterjet or hydraulic cutting (fig. 4.6, *a*) and abrasive waterjet cutting (fig. 4.6, *b*). Waterjet cutting is used for shaped cutting of foam, rubber, cardboard, leather, paronite, cork, industrial cloth, and other similar non-metallic materials. Waterjet cutting is used for production of details of any steels (structural, high-tensile, high-temperature), non-ferrous metals and alloys (titanium and titanium alloys, aluminium alloys, cupper, bronze), and also for production of details of glass, organic glass, composite materials, plastic, ceramic, graphite, natural and reconstructed stone (marble, granite, ceramic granite).

An abraser in the jet increases its technological properties, and the liquid-abrasive suspension can be used for cutting hard and refractory materials with great thickness. The waterjet cutting modes for both methods can be expanded by inputting

a cooling agent to the jet head, which intensifies formation of ice particle in the jet imparting abrasive properties to it [82].

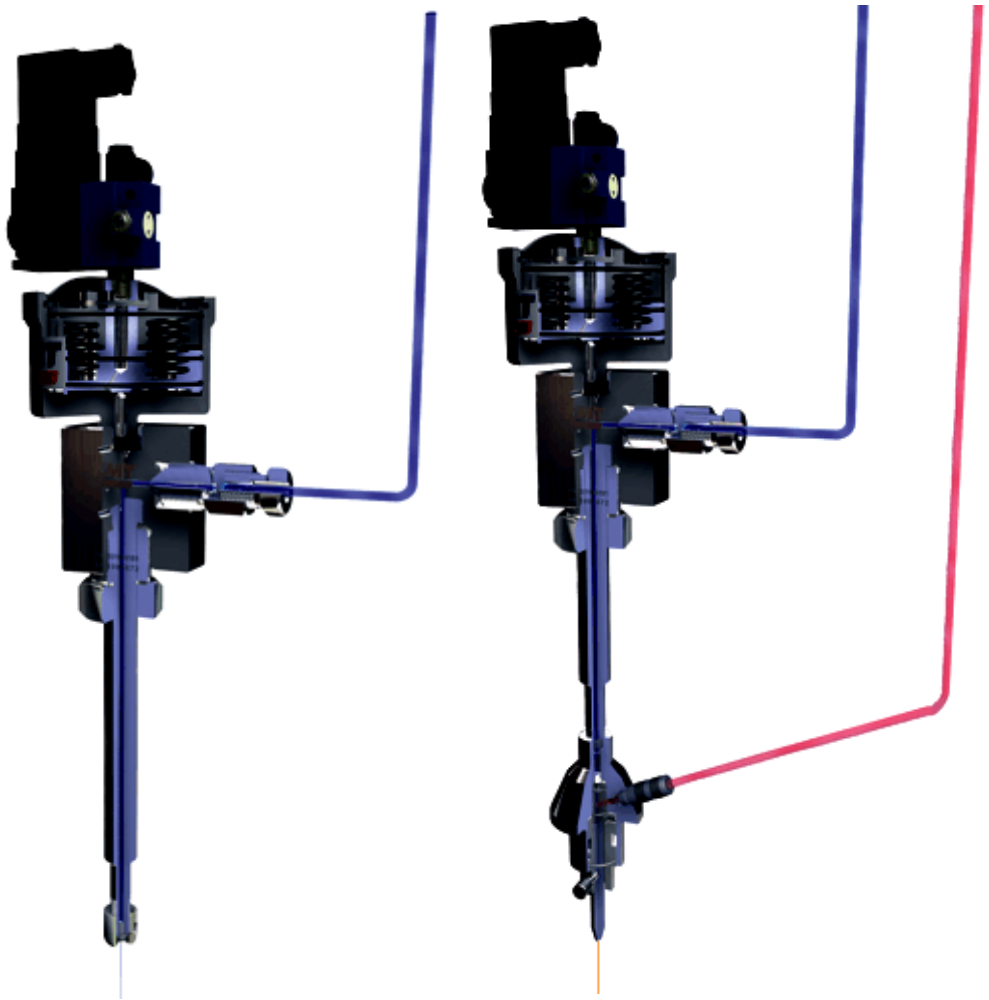

a *b*

Figure 4.6 – Water jet cutter (*a*) and abrasive water jet cutter (*b*)

Abrasive and erosion wears, impacts, corrosion, cavitation, combined wear, and friction wear are factors that greatly affect the service life and decrease the operational resource of the expensive equipment, including that for hydro-abrasive treatment of materials. Therefore, still urgent is the issue of development of low-cost and wear-resistant materials for the tube, because these characteristics are needed to form the smooth and directed cutting jet ensuring efficient abrasive waterjet cutting. Fig. 4.7 gives the diagram and picture of the cutting head for AWJ.

The material designed on the basis of zirconium dioxide and partially stabilized with yttrium oxide with additives of tungsten carbide is recommended for manufacturing the focusing tube of nozzles for hydraulic and hydro-abrasive treatment (hereafter – tubes).

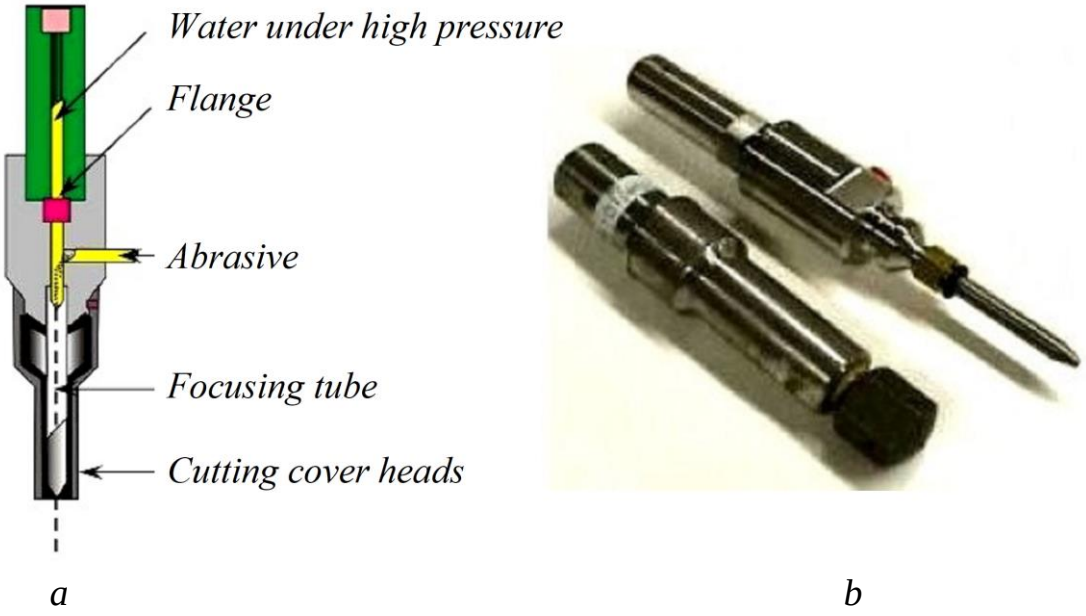

Figure 4.7 – Diagram (*a*) and photo (*b*) of the cutting head for AWJ

Sapphire and hard alloy are the most widespread materials for tubes used for the waterjet cutting of metals where high strength characteristics due to application of high working pressures (up to 140 MPa) are required. Each material type has certain advantages and disadvantages under different operational conditions. The production quality and the service life are critical parameters of tubes.

Sapphire tubes are frequently used for working pressures over 140 MPa. They generate high-quality jet if an outlet size is less than 1 mm, but they have the worst jet quality if the sizes are large in comparison with hard-alloyed and steel tubes. Sapphire tubes must be used for very pure water distilled to 10 mkm and higher. Under good operational conditions their service life can reach 200 hours and longer, as the material does not suffer from erosion, which is typical for hard-alloyed and corundum nozzles. Nonetheless, sapphire is a very brittle material and any small fraction along the tube edge will considerably impact the jet quality. Any particle in the water going through the nozzles will cause such fractions and, if a great amount of particles enters the sapphire tube this causes immediate cracking. Besides, such sapphire tubes can also be easily damaged with fragments of the spent material. All the mentioned-above properties and high cost of such tubes restrict their wide application for AWJ.

Hard alloy is frequently considered strongest among all materials for tubes. For dirty undistilled water they are most durable. The material of hard alloy tubes consists of wolfram carbide with bonding. The amount and type of a binding agent in hard alloy can vary, and these variables affect the strength and stability of the erosion tube. The comparative testing was made for tubes of the designed composition of ZrO_2–

20 mass% WC with the highest coefficient of fracture viscosity and hardness, and of hard VK3 low-cobalt alloy and the VK15 average-cobalt alloy (table 4.4). The speed and the wear type were also studied.

Table 4.4 – Tubes used in testing on wear resistance

Material of the tube		Tube size $L \times D_{in} \times D_{out}$, mm	Manufacturer
Composition 1	ZrO_2–20 mass% WC	70×6.35×1.0	–
Composition 2	VK3		Kennametal (Germany)
Composition 3	VK15		Lidun (China)

It was found that the tubes of composition 1 demonstrated the typical erosion wear with obvious homogeneity along the whole tube surface and the outlet section increases regularly while the nozzle is still generating a directed jet. In this case the outlet diameter increases by 0.1 mm, which results in low speed of the flame by 20 %. However, the change in the diameter by this value for the tube with a 2.0 mm opening causes an increase in the expenses only by 10 %. Fig. 4.8 demonstrates a change in the outlet diameter for different material types, and fig. 4.9 presents the jet samples obtained for each composition after the 80-hour testing.

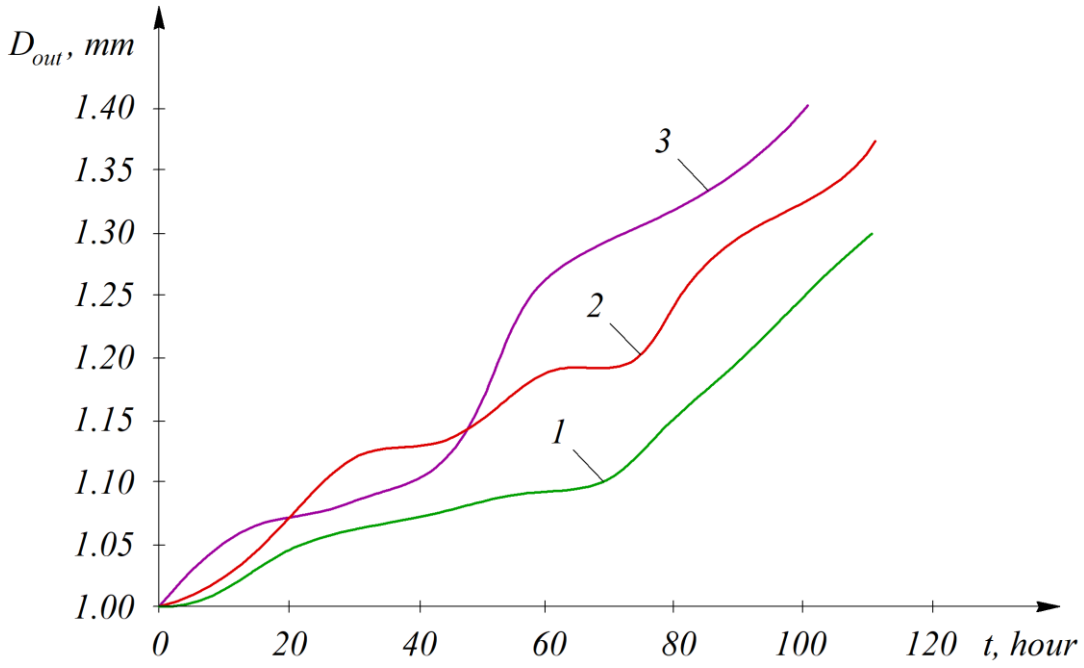

Figure 4.8 – Dependency of a change in the outlet diameter on the running time for tubes of different materials:
1 – composition 1; *2* – composition 2; *3* – composition 3

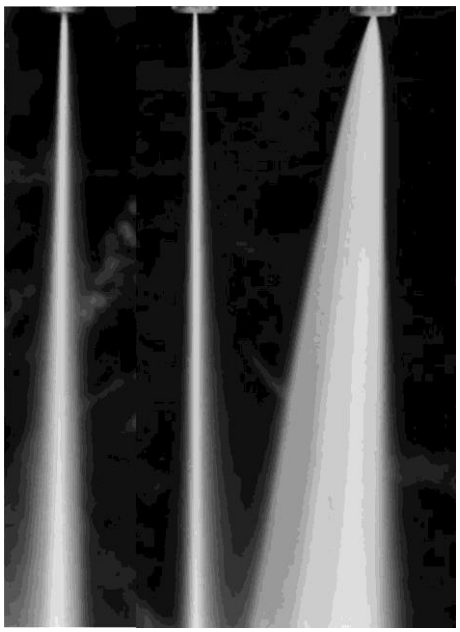

a *b* *c*

Figure 4.9 – Samples of the jet going out of the tubes of composition 2 (*a*), composition 1 (*b*) and composition 3 (*c*) after the 80-hour testing

The channel surface of the tube of composition 1 after 80 running hours (fig. 4.10, *a*) has the homogeneous structure unlike its surface structure, but after 110 running hours (fig. 4.10, *b*) the center of intensive heterogeneous erosive wear in the form of voids in the material can clearly be seen, which directly decreases the jet quality.

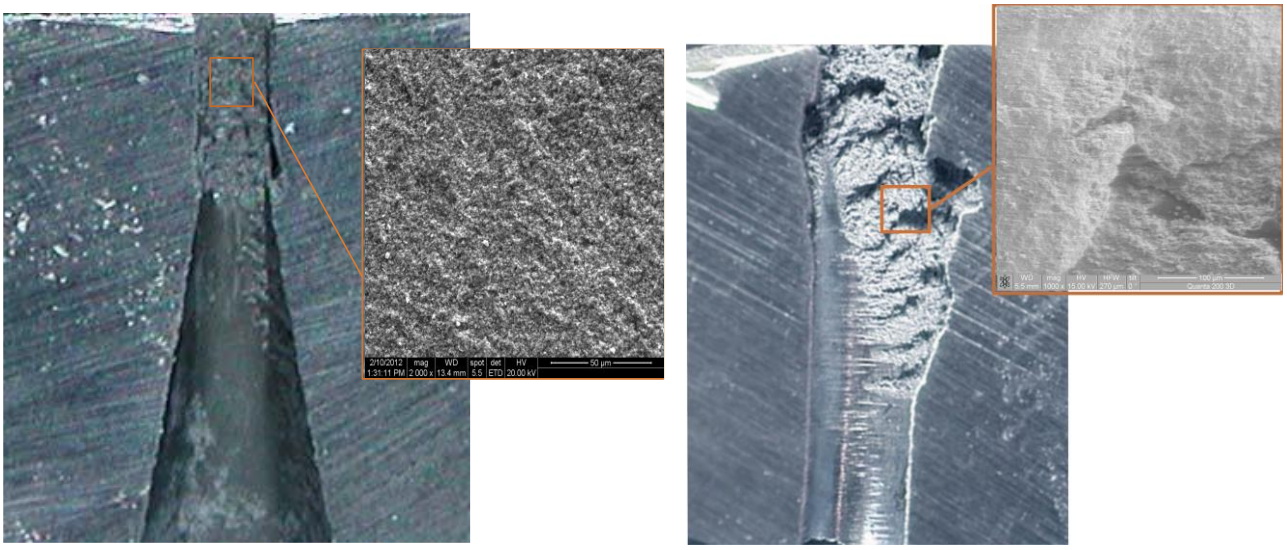

a *b*

Figure 4.10 – Pattern of the wear surface on the tube of composition 1 after 80 hours (*a*) and 110 hours (*b*) of work

It has been found that for compositions 2 and 3 the failures in the tubes occur if erosion develops unevenly and the outlet sizes slightly change, however, it is the jet quality that is affected more. In these cases the tube wear implies the lower productivity, and the cutting power of jet decreases, besides the tube of composition 3 failed to function much earlier than the tube of composition 2. Most likely, this fact is explained by higher amount of a binding agent in the average-cobalt alloy (composition 3), consequently, the number of contacts between the tungsten carbide particles decreases, and the erosion process runs quicker, than that in composition 2, where the cobalt phase concentration in the fracture process is insignificant due to its small areal part.

As known, at first, in the solid alloy the cobalt phase is fractured and eliminated. Thus, the wear mechanism in hard-alloyed tubes includes erosion of the binding agent in combination with corrosion erosion. The research has demonstrated that regular distribution of the tungsten carbide additive in the composite volume, provided as early as at the stage of fabricating powders, and a small grain size in the material, achieved due to the optimal electroconsolidation modes, explains a longer service life of tubes produced of the material developed if compare them with those of hard alloyed material.

The longer service life of nozzles of composition 1 can be explained by the same mechanisms. As known, in brittle materials due to their low deformation capacity large fragments of the material are separated from the wear surface by creating micro cracks with their further development. However, in the material of composition 1 such cracks meet tungsten carbide grains with higher elasticity modulus than that of zirconium dioxide. And the cracks have either to bend around or break them into smaller components. This causes spending additional energy or increasing deformation efforts. This fact together with high hardness and the capacity of zirconium dioxide to martensitic transformation in the stress field near the crack growing, which, in turn, causes considerable solidification of the material, provides the high strength of the developed composition 1 during abrasive and erosion effects.

A prospective approach is application of submicron composites based on zirconium oxide with additives of tungsten carbide for other goods working under the conditions of abrasive and erosion wear, for example, the material for amplifying Venturi nozzles, the material for the internal profile of the systems for elimination of abrasive product (oxide film) in powerful steam turbines, the material for discharges and elements of the wet ends of aligned pumps, which are prone to cavity-abrasive wear.

REFERENCES

1. Mashkov, Yu. K., Malii, O. V. (2014). Materialy i metody nanotekhnologii. Omsk: Izdatel'stvo OmGTU, 136.

2. Chyshkala, V. O., Lytovchenko, S. V., Nerubatskyi, V. P., Vovk, R. V., Gevorkyan, E. S., Morozova, O. M. (2022). Detection of regularities of $Y_2Zr_2O_7$ pyrochlor phase formation during the reaction of solid-phase synthesis under different temperature-time conditions. *Functional Materials*, 29, 1, 30–38. DOI: 10.15407/fm29.01.30.

3. Chyshkala, V. O., Lytovchenko, S. V., Gevorkyan, E. S., Nerubatskyi, V. P., Morozova, O. M. (2021). Structural phase processes in multicomponent metal ceramic oxide materials based on the system Y–Ti–Zr–O (Y_2O_3–TiO_2–ZrO_2). *SWorldJournal*, 7, 1, 17–32. DOI: 10.30888/2663-5712.2021-07-01-008.

4. Keramicheskie materialy. (1991). Pod red. G. N. Maslennikovoi. Moskva: Stroiizdat, 320.

5. Mal'tsev, A. N. (2006). Sverkhtverdye nanosplavy. *V mire nauki*, 2, 12–15.

6. Zeiler, B. A. (1997). Low cost method for pressure–assisted densification of advaced materials into complet shaped parts in. *Proceedings of the 14th International Plansee Seminar*, 4, 265–276.

7. Gevorkyan, E. S., Semchenko, G. D., Timofeeva, L. A., Nerubatskyi, V. P. (2015). New materials and technologies for their production: textbook. Kharkiv: “Disa plyus”, 344.

8. Andrievskii, R. A. (2005). Nanomaterialy na osnove tugoplavkikh karbidov, nitridov i boridov. *Uspekhi khimii*, 12, 1163–1175.

9. Fesenko, I. P., Kislii, P. S., Kuzenkova, M. O., Oleinik, G. D. (2002). Keramika z nanoporoshku AlN. *Sverkhtverdye materialy*, 4, 48–54.

10. Pshenichnaya, O. V. (2002). Poluchenie nanokristallicheskikh kompozitsionnykh poroshkov azotirovaniem alyuminidov titana i tsirkoniya. *Sverkhtverdye materialy*, 2, 59–63.

11. Gevorkyan, E., Prokopiv, M., Rucki, M., Morozow, D. (2019). Durability and exploitation performance of cutting tools made out of chromium oxide nanocomposite materials. *Eksploatacja i Niezawodnosc – Maintenance and Reliability*, 21, 4, 686–691. DOI: 10.17531/ein.2019.4.19.

12. Gevorkyan, E., Nerubatskyi, V., Chyshkala, V., Gutsalenko, Y., Morozova, O. (2021). Determining the influence of ultra-dispersed aluminum nitride impurities on the structure and physical-mechanical properties of tool ceramics.

Eastern-European Journal of Enterprise Technologies, 6, 12 (114), 40–52. DOI: 10.15587/1729-4061.2021.245938.

13. Birringer, R., Gleiter, H., Marquard, P. (1984). Nanocrystalline materials: an approach to novel solid structure with gas–like disorder. *Phys. Lett.*, 102, 365–369.

14. Gevorkyan, E., Nerubatskyi, V., Chyshkala, V., Morozova, O. (2021). Revealing specific features of structure formation in composites based on nanopowders of synthesized zirconium dioxide. *Eastern-European Journal of Enterprise Technologies*, 5, 12 (113), 6–19. DOI: 10.15587/1729-4061.2021.242503.

15. Gevorkyan, E. S., Rucki, M., Kagramanyan, A. A., Nerubatskiy, V. P. (2019). Composite material for instrumental applications based on micro powder Al_2O_3 with additives nano-powder SiC. *International Journal of Refractory Metals and Hard Materials*, 82, 336–339. DOI: 10.1016/j.ijrmhm.2019.05.010.

16. Andrievskii, R. A. (2003). In Processing and properties of nanocrystalline materials. *J. Material Science*, 38, 1367–1380.

17. Andrievskii, R. A. (2002). Termicheskaya stabil'nost' nanomaterialov. *Uspekhi khimii*, 71, 10, 967–981.

18. Gevorkyan, E. S., Rucki, M., Nerubatskyi, V. P., Żurowski, W., Siemiątkowski, Z., Morozow, D., Kharatyan, A. G. (2022). Remanufacturing and advanced machining processes for new materials and components. Taylor & Francis, 204. DOI: 10.1201/9781003218654.

19. Gevorkyan, E., Nerubatskyi, V., Gutsalenko, Yu., Melnik, O., Voloshyna, L. (2020). Examination of patterns in obtaining porous structures from submicron aluminum oxide powder and its mixtures. *Eastern-European Journal of Enterprise Technologies*, 6, 6 (108), 41–49. DOI: 10.15587/1729-4061.2020.216733.

20. Gevorkyan, E. S., Nerubatskyi, V. P., Gutsalenko, Yu. H., Morozova, O. M. (2020). Some features of ceramic foam filters energy efficient technologies development. *Modern engineering and innovative technologies*, 14, 1, 46–60. DOI: 10.30890/2567-5273.2020-14-01-014.

21. Gevorkyan, E., Rucki, M., Nerubatskyi, V., Siemiatkowski, Z., Morozow, D., Komarova, H. (2022). Theoretical model of the densification during hot pressing and its verification. *In: Gapiński, B., Ciszak, O., Ivanov, V. (eds) Advances in Manufacturing III. Manufacturing 2022. Lecture Notes in Mechanical Engineering*. Springer, Cham, 113–123. DOI: 10.1007/978-3-031-00805-4_10.

22. Gevorkyan, E. S., Nerubatskyi, V. P. (2009). The question of obtaining finely dispersed structures from aluminum oxide nanopowders. *Collected scientific works of Ukrainian State Academy of Railway Transport*, 111, 151–167.

23. Groza, J. R. (1998). Field assited sintering. *Powder Metallurgy*, 7, 2, 583–589.

24. Nersisyan, H. H., Lee, J. H., Won, C. W. (2003). SHS for a large-scale synthesis method of transition metal nanopowders. *Int. J. Self-Propag. High-Temp. Senth.*, 12, 149–158.

25. Groza, J. R. (2002). Consolidation of nanocrystalline powders in Nanostructured Materials. *Powder Metallurgy*, 5, 10, 115–178.

26. Groza, J. R., Zavaliangos, A. K. (2000). Sintering activation by external electrical field. *Material Scince*, 28, 171–177.

27. Rifcin, J. A. (1998). Nanoparticale sintering simulation. *Mater. Sci. Eng.*, 252, 1489–1496.

28. Groza, J. R., Curtis, J. D., Kramer, M. (2000). Field assited sintering of nanocrystalline titanium nitride. *J. American Ceramic Society*, 85, 5, 1281–1283.

29. Goldberger, W. M. (1998). Using silicon carbide in advanced ceramics. *Ceramic Industry*, 148, 6, 68–72.

30. Goldberger, W. M., Fessler, R. R. (1999). The development of non-intrusive methods of sencing and control of densification during electrocosolidation. *Advances in Process Measurments for the Ceramic Industry*, 18, 42, 337–345.

31. Gevorkyan, E. S., Nerubatskyi, V. P., Chyshkala, V. O., Morozova, O. M. (2020). Aluminum oxide nanopowders sintering at hot pressing using direct current. *Modern scientific researches*, 14, 1, 12–18. DOI: 10.30889/2523-4692.2020-14-01-002.

32. Skorokhod, V. V., Uvariva, I. V., Ragulya, A. V. (2001). Fiziko-khimichna kinetika v nanostrukturnikh sistemakh. Kyiv: Akademperiodika, 180.

33. Johnson, D.L. (1989). Ultra-rapid sintering of ceramics. In: Uskoković, D. P., Palmour, H., Spriggs, R. M. (eds) Science of Sintering. Springer, Boston, MA. DOI: 10.1007/978-1-4899-0933-6_44.

34. Gevorkyan, E., Mamalis, A., Vovk, R., Semiatkowski, Z., Morozow, D., Nerubatskyi, V., Morozova, O. (2021). Special features of manufacturing cutting inserts from nanocomposite material Al_2O_3-SiC. *Journal of Instrumentation*, 16, 10, P10015. DOI: 10.1088/1748-0221/16/10/P10015.

35. Cao, T., Li, X., Li, J., Huang, Y., Qu, S., Yang, C., Liang, L., Song, T. (2021). Mechanical properties of WC-Si_3N_4 composites with ultrafine porous boron nitride nanofiber additive. *Frontiers in Materials*, 8, 534407. DOI: 10.3389/fmats.2021.534407.

36. Gevorkyan, E. S., Vovk, R. V., Sofronov, D. S., Nerubatskyi, V. P., Morozova, O. M. (2021). The composite material based on synthesized zirconium

oxide nanopowder for structural appliance. *17th International Conference on Advanced Nanomaterials* (July 22–24, 2021, Aveiro, Portugal), 267.

37. Gevorkyan, E. S., Nerubatskyi, V. P., Morozova, O. M., Chyshkala, V. A., Sofronov, D. S., Meshcheriakova, O. P. (2021). Technical ceramics based on zirconia dioxide. *Reports of the IX International Scientific-Practical Conference "A Person, a Society, Communicative Technologies"* (October 21–22, 2021, Kharkiv, Ukraine). Kharkiv: TOV "Disa plyus", 257–259.

38. Kamagaito, N. (1991). What can be improved by nanometer composites. *J. Jpn. Soc. Powder Metall.*, 38, 315–321.

39. Khasanov, O. L. (2003). Metody izgotovleniya i svoistva VTSP-keramiki na osnove ul'tradispersnykh poroshkov. *Izvestiya Tomskogo politekhnicheskogo universiteta,* 306, 3, 61–66.

40. Semchenko, G. D. (2002). Sovremennye protsessy v tekhnologii keramiki: Uchebnoe posobie. Khar'kov: NTU "KhPI", 80.

41. Vovk, R. V., Gevorkyan, E. S., Nerubatskyi, V. P., Prokopiv, M. M., Chyshkala, V. O., Melnyk, O. M. (2018). New ceramic composite materials for instrumental purposes: monograph. Kharkiv: V. N. Karazin Kharkiv National University, 200.

42. Gevorkyan, E. S., Nerubatskyi, V. P., Chyshkala, V. O., Morozova, O. M. (2021). Cutting composite material based on nanopowders of aluminum oxide and tungsten monocarbide. *Modern engineering and innovative technologies*, 15, 2, 6–14. DOI: 10.30890/2567-5273.2021-15-02-020.

43. Besson, J. R., Abouaf, M. S. (1992). The sintering behavior of ultrafine alumina particles. *Journal of Materials Research,* 7, 1489–1493.

44. Dutka, V. A., Pereyaslov, V. P., Ivanov, S. A., Bologova, L. M. (2006). Chisel'nii analiz vplivu konstruktsiï tekhnologichnogo vuzla ta rezhimu nagrivannya na temperaturu robochogo sharu pri napikanni iogo na korpus burovoï koronki. *Sverkhtverdye materialy*, 2, 72–83.

45. Zigel', R., Khauell, Dzh. (1975). Teploobmen izlucheniem. Moskva: Mir, 935.

46. Greenberg, D. P., Cohen, M. F., Torrance, K. E. (1986). Radiosity: a method for computing global illumination. *The Visual Computer,* 2, 291–297.

47. Vanmeensel, K., Laptev, A., Hennicke, J., Vleugels, J., Van der Biest, O. (2005). Modelling of the temperature distribution during field assisted sintering. *Acta Materialia,* 53, 4379–4388. DOI: 10.1016/j.actamat.2005.05.042.

48. Muñoz, S., Anselmi-Tamburini, U. (2013). Parametric investigation of temperature distribution in field activated sintering apparatus. *The International*

Journal of Advanced Manufacturing Technology, 65, 127–140. DOI: 10.1007/s00170-012-4155-7.

49. Denisov, M. A. (2011). Matematicheskoe modelirovanie teplofizicheskikh protsessov: ANSYS i CAE-proektirovanie. Ekaterinburg: UrFU, 149.

50. Zubchenko, A. S. (2003). Marochnik stalei i splavov. 2-e izd., pererab. i dop. Moskva: Mashinostroenie-1, 784.

51. Fiziko-khimicheskie svoistva okislov: Spravochnik. (1978). Pod red. G. V. Samsonova. Moskva: Metallurgiya, 472.

52. Teplo- i massoobmen. Teplotekhnicheskii eksperiment: Spravochnik. (1982). Pod obshch. red. V. A. Grigor'eva i V. I. Zorina. Moskva: Energoizdat, 510.

53. Wei, X., Giuntini, D., Maximenko, A. L., Haines, C. D., Olevsky, E. A. (2015). Experimental investigation of electric contact resistance in spark plasma sintering tooling setup. *Journal of the American Ceramic Society,* 8, 2, 3553–3560. DOI: 10.1111/jace.13621.

54. Rothe, S., Kalabukhov, S., Frage, N., Hartmann, S. (2016). Field assisted sintering technology. Part I: Experiments, constitutive modeling and parameter identification. *GAMM-Mitt*, 39, 2, 114–148.

55. Zavaliangos, A., Zhang, J., Krammer, M., Groza, J. R. (2004). Temperature evolution during field activated sintering. *Materials Science and Engineering: A,* 379, 1–2, 218–228. DOI: 10.1016/j.msea.2004.01.052.

56. Tablitsy fizicheskikh velichin: Spravochnik. (1976). Pod. red. akad. I. K. Kikoina. Moskva: Atomizdat, 1008.

57. Nikolaenko, A. N. (1996). Statisticheskii analiz raspredeleniya poroshkov v svobodnoi zasypke. *Poroshkovaya metallurgiya,* 2, 79–82.

58. Suryanarayanan Iyer, R., Sastry, S. M. L. (1999). Consolidation of nanoparticles – development of a micromechanistic model. *Acta Materialia,* 47, 10, 3079–3098. DOI: 10.1016/S1359-6454(99)00116-0.

59. Ur'ev, N. B. (1975). Fiziko-khimicheskaya mekhanika v tekhnologii dispersnykh sistem. Moskva: Znanie, 64.

60. Kim, H.-C., Shon, I.-J., Yoon, J.-K., Doh, J.-M. (2007). Consolidation of ultra fine WC and WC–Co hard materials by pulsed current activated sintering and its mechanical properties. *International Journal of Refractory Metals and Hard Materials,* 25 (1), 46–52. DOI: 10.1016/j.ijrmhm.2005.11.004.

61. Frost, G. D., Eshbi, M. F. (1989). Karty mekhanizmov deformatsii. Chelyabinsk: Metallurgiya, 230.

62. Besson, J. R., Abouaf, M. S. (1992). *Journal of Materials Research,* 7, 6, 1489–1500. DOI: 10.1557/JMR.1992.1489.

63. Kurdyumov, A. V. (2000). Sintez i struktura nanodispersnykh poroshkovykh sverkhtverdykh faz. *Poroshkovaya metallurgiya,* 7–8, 47–54.

64. Kwon, Y.-S., Gromov, A. A., Strokova, J. I. (2007). Passivation of the surface of aluminum nanopowders by protective coatings of the different chemical origin. *Applied Surface Science,* 253 (12), 5558–5564. DOI: 10.1016/j.apsusc.2006.12.124.

65. Andrievski, R. A. (2000). New nanocrystaline materials. *In Advanced Science and Technology of Sintering.* Kluwer Academic, Dordrecht, 204–209.

66. Guicciardi, S. (1999). Composition dependence of mechanical and wear properties of electroconductive ceramics. *Poroshkovaya metallurgiya,* 3–4, 32–41.

67. Gevorkyan, E. S., Nerubatskyi, V. P. (2009). Modeling of the AL_2O_3 hot pressing process with direct transmission of an alternating electric current with a frequency of 50 Hz. *Collected scientific works of Ukrainian State Academy of Railway Transport,* 110, 45–52.

68. Raichenko, A. I. (1987). Osnovy protsessa spekaniya poroshkov propuskaniem elektricheskogo toka. Moskva: Metallurgiya, 128.

69. Raichenko, A. I. (1979). Nekotorye osobennosti elektrospekaniya poroshkov. *Poroshkovaya metallurgiya,* 8, 27–31.

70. Raichenko, A. I., Istomina, T. I., Troyan, I. A. (2000). Spekanie poroshkov pri nalozhenii elektricheskogo toka i periodicheskikh mekhanicheskikh impul'sov. *Poroshkovaya metallurgiya,* 3–4, 105–109.

71. Stanciu, L. A., Kodash, V. Y., Groza, J. R. (2001). Effects of heating rate on densification and grain growth during field-assisted sintering of α-Al_2O_3 and $MoSi_2$ powders. *Metallurgical and Materials Transactions A,* 32 (10), 2633–2638. DOI: 10.1007/s11661-001-0053-6.

72. German, R. M. (1996). Sintering theory and practice. 568.

73. Anderson, K. R., Groza, J. R., Fendorf, M., Echer, C. J. (1999). Surface oxide bonding in field assited powder sintering. *Materials Science & Engineering*, 270, 2, 278–282.

74. Gevorkyan, E., Rucki, M., Krzysiak, Z., Chishkala, V., Zurowski, W., Kucharczyk, W., Barsamyan, V., Nerubatskyi, V., Mazur, T., Morozow, D., Siemiątkowski, Z., Caban, J. (2021). Analysis of the electroconsolidation process of fine-dispersed structures out of hot pressed Al_2O_3–WC nanopowders. *Materials*, 14, 21, 6503. DOI: 10.3390/ma14216503.

75. Gevorkyan, E., Rucki, M., Sałaciński, T., Siemiątkowski, Z., Nerubatskyi, V., Kucharczyk, W., Chrzanowski, Ja., Gutsalenko, Yu., Nejman, M.

(2021). Feasibility of cobalt-free nanostructured WC cutting inserts for machining of a TiC/Fe composite. *Materials*, 14, 12, 3432. DOI: 10.3390/ma14123432.

76. Kroke, E., Li, Y.-L., Konetschny, C., Lecomte, E., Fasel, C., Riedel, R. (2000). Silazane derived ceramics and related materials. *Materials Science and Engineering: R: Reports,* 26 (4–6), 97–199. DOI: 10.1016/s0927-796x(00)00008-5.

77. Groza, J. R., Garcia, M., Schneider, J. A. (2001). Surface effects in field-assisted sintering. *Journal of Materials Research,* 16 (01), 286–292. DOI: 10.1557/jmr.2001.0043.

78. Mikolaєnko, A. M. (1996). Statistichnii analiz strukturi randomizovannogo ustatkuvannya v seredovishchi dribnikh chastin. *Ukraïns'kii fizichnii zhurnal,* 2, 243–250.

79. Kislyi, P. S., Bodnaruk, N. I., Gorichok, Ya. O. (1986). Fiziko-khimicheskie osnovy polucheniya tugoplavkikh sverkhtverdykh materialov. Kiev: Naukova dumka, 208.

80. Novikov, N. V. Grabchenko, A. I. Gritsenko, E. I. (1988). Lezviinyi instrument iz sverkhtverdykh materialov: Spravochnik. Pod red. N. V. Novikova. Kiev: Tekhnika, 118.

81. Gevorkyan, E. S., Kodash, V. Yu., Kramer, M. (2004). Issledovanie rezhushchikh svoistv razlichnykh instrumental'nykh materialov pri obrabotke Ferrotitanita–S. Visoki tekhnologiї v mashinobuduvanni: *Zbirnik naukovikh prats' NTU "KhPI",* 2 (a), 59–64.

82. Gevorkyan, E. S., Timofeeva, L. A., Nerubatskyi, V. P., Melnyk, O. M. (2016). Integrated technologies of materials processing: textbook. Kharkiv: USURT, 238.

Scientific publication

GEVORKYAN Edwin Spartakovych
NERUBATSKYI Volodymyr Pavlovych

TECHNOLOGICAL AND SCIENTIFIC ASPECTS OF CONSOLIDATION OF REFRACTORY COMPOSITES

Monograph

Responsible for release Nerubatskyi V. P.

Author's edition

Sent to the printer 25.05.2022. Format 60×84/16.
Type Times New Roman. Offset paper.
Printer’s sheet 4.78. 50 printed copies. Order № 121408. Agreed price.

Publisher LLC “VOSKHOD-PRINT”
61057, Kharkiv, Rymars′ka str., 3/5

Manufacturer Individual person-entrepreneur Machulin L. I.
61057, Kharkiv, Rymars′ka str., 3/5
Certificate ХК № 125 of 24.11.2004